Lab on a Chip

CRITICAL REVIEW

View Article Online
View Journal | View Issue

Cite this: *Lab Chip*, 2023, **23**, 1467

Recent progress in nucleic acid detection with CRISPR

Frank X. Liu,[a] Johnson Q. Cui,[a] Zhihao Wu [b] and Shuhuai Yao *[ac]

Received 4th October 2022,
Accepted 20th January 2023

DOI: 10.1039/d2lc00928e

rsc.li/loc

Recent advances in CRISPR-based biotechnologies have greatly expanded our capabilities to repurpose CRISPR for the development of molecular diagnostic systems. The key attribute that allows CRISPR to be widely utilized is its programmable and highly specific nature. In this review, we first illustrate the principle of the class 2 CRISPR nucleases for molecular diagnostics which originates from their immunologic defence systems. Next, we present the CRISPR-based schemes in the application of diagnostics with amplification-assisted or amplification-free strategies. By highlighting some of the recent advances we interpret how general bioengineering methodologies can be integrated with CRISPR. Finally, we discuss the challenges and exciting prospects for future CRISPR-based biosensing development. We hope that this review will guide the reader to systematically learn the start-of-the-art development of CRISPR-mediated nucleic acid detection and understand how to apply the CRISPR nucleases with different design concepts to more general applications in diagnostics and beyond.

1 Introduction

Detection of nucleic acids is of great importance for the identification of genetic diseases and pathogenic diagnosis, as well as its use in therapeutics. In recent decades, large-scale recurring disease outbreaks caused by emerging viruses, such as SARS, H1N1, Ebola, Zika, and SARS-CoV-2,[1] highlight that the current gold standard approach polymerase chain reaction (PCR), which requires centralized diagnostic facilities, is unable to respond quickly to these pandemic or epidemic crises. The response time is significantly delayed by sample collection, transport, preparation, and slow reaction time. As guided by the World Health Organisation (WHO), the ideal pathogen detection should be affordable, sensitive, specific, user-friendly, rapid and robust, equipment-free, and deliverable to end-users (ASSURED). Therefore, there is an urgent need for deployable and miniaturized point-of-care testing (POCT) platforms to address viral detection.

Over the past few years, the emerging clustered regularly interspaced short palindromic repeats (CRISPR) technology has revolutionized the field of gene editing and molecular diagnostics.[2] Originally, the CRISPR–Cas system was a prokaryotic adaptive immune system used against viruses and plasmids in most archaea and bacteria.[3] In the immune system, the CRISPR array inserts a portion of the target DNA sequence next to the protospacer adjacent motif (PAM) sequence to become a spacer where the CRISPR array is transcribed as a single transcript containing the spacer sequence and parts of the flanking repeats.[4] The CRISPR RNA (crRNA) coupled with Cas nucleases recognizes the protospacer sequence in the invading objects, then the invading viruses or plasmids are cleaved and deactivated by the Cas nucleases.[5–9] Although this was first discovered in the 1980s,[10] it was not until 2012 that the first *in vitro* demonstration of an engineered Cas9 system was used to specifically cut the targeted sequence by fusing RNA molecules into a single-guide RNA (sgRNA).[11] By programmable design of the spacer of the sgRNA, the CRISPR coupled with Cas effectors offer unparalleled potential for genome-editing applications such as sequencing and molecular diagnostics.[11–16] The subsequent discovery of the *cis* and *trans*-cleavage ability of Cas12 and Cas13 has shown more values in molecular diagnostics where Cas proteins *trans*-cleave the surrounding single-stranded reporters after the *cis* base-pair matching between the guided RNA spacer and targeted protospacer sequences. The applications of the CRISPR toolbox in molecular diagnostics imply its merits as follows: (i) programmable and easy to design, (ii) near-ambient operational temperature, and (iii) high sensitivity to single mutation variants.

The first diagnostic application of CRISPR was reported in 2016. With the preamplification of NASBA, the Cas9 achieved

[a] *Department of Mechanical and Aerospace Engineering, Hong Kong University of Science and Technology, Clear Water Bay, Kowloon, Hong Kong. E-mail: meshyao@ust.hk*
[b] *IIP-Advanced Materials, Interdisciplinary Program Office (IPO), Hong Kong University of Science and Technology, Clear Water Bay, Kowloon, Hong Kong*
[c] *Department of Chemical and Biological Engineering, Hong Kong University of Science and Technology, Clear Water Bay, Kowloon, Hong Kong*

superior specific and sensitive detection of the Zika virus at a single nucleotide polymorphism (SNP).[12] In the same year, the collateral activity of Cas13a was reported,[17] and employed for direct RNA detection without amplification.[18] The amplification-associated and amplification-free detection ability of trace amounts of nucleic acids by the CRISPR–Cas system has since been harnessed for the next generation of nucleic acid detection. The CRISPR-driven diagnostic tools have been intensively developed as an alternative to the PCR test. Several of these tools including LAMP-DETECTR and LAMP-SHERLOCK have been approved by the US Food Drug Administration (FDA).[19]

CRISPR-mediated molecular diagnostics has been a hot topic in recent reviews.[20–29] These review papers provide different aspects of recent advances in CRISPR diagnostic technologies including understanding the cellular biology of CRISPR and principles for diagnostics,[20,22,24] the transition of CRISPR technology to molecular diagnostics from tube to device for POCT,[27,29] strategies and technologies that can be coupled with CRISPR such as microfluidics and nanotechnologies,[23,25] and the application for COVID-19 diagnostics to meet the urgent pandemic emergency.[21,28] Nevertheless, the design principles of how the CRISPR effectors work with different strategies and technologies to meet the sensing and quantification demands have not been elaborated and clearly outlined. More importantly, with the continuous expansion of CRISPR-based tools in the past few years, it is important to summarize and update new working principles and trends of this field. In this review, we tend to focus on the selection preference of Cas effectors, amplification methods, and reporting schemes. We summarize the development of CRISPR-based diagnostics in two main categories in coupling with nucleic acid amplification-assisted and amplification-free (signal amplification) techniques, respectively. With the aid of theory and examples, we present a synthesized overview from the design principles to the detection techniques in detail to illustrate how different CRISPR effectors can be integrated with nucleic acid detection protocols.

The review is structured as follows: first, we provide a short summary of the mechanisms and characteristics of class 2 CRISPR–Cas systems including conjugation strategies and cleavage purposes that guide the design concepts. Second, we summarize the isothermal preamplification schemes associated with CRISPR, illustrating the advantages and disadvantages of these methods in different scenarios (Tables 3–5). Third, we review the amplification-free (*i.e.*, without polymerase adoption) assays in combination with CRISPR indicating that the CRISPR systems are promising for facile detection without target molecule amplification (Table 6). Lastly, from CRISPR implementation theory to diagnostic applications, we highlight advanced functions of CRISPR for quantitative, multiplexed, and all-in-one diagnostic purposes, and present our views on the outstanding issues and potential solutions regarding how to make the detection schemes fit for specific scenarios and how to simplify the sample-in and results-out procedures toward POCT. We hope that this review will guide the reader to choose their adventure of CRISPR-based diagnostics with either amplification-assisted or amplification-free methods for specific applications.

2 CRISPR classification and diagnostic mechanisms

As various CRISPR–Cas systems have been discovered, they have been categorized into two classes (class 1 and class 2) depending on whether it is a single protein effector during the interference process. While the class 1 nucleases use multiple proteins as an effector complex for the interference function, the class 2 enzymes rely on a single protein effector during the interference process such as the families of Cas9, Cas12, and Cas13. The details of the hierarchical categorization can be found in ref. 9. To date, most of the nucleic acid and associated molecular diagnostics are based on the class 2 CRISPR family with a few exceptions.[30,31] Moreover, different variants have shown notable differences in terms of PAM sequences, sensitivity, and cleavage loci, offering more options for the CRISPR diagnostic toolbox. Therefore, we summarize the commonly used Cas proteins according to their features, such as origins, PAM/protospacer flanking site (PFS) sequences, target type, and sensitivity (the sensitivity here was measured by previous research using fluorescence without amplification) in Table 1. Santiago's group has investigated the sensitivity of some of those listed enzymes using Michaelis–Menten enzyme kinetics theory systematically,[32–34] showing that the sensitivity of those enzymes is governed by enzymatic kinetics. Among all the identified enzymes, the reaction temperature of the enzymes was found to be around 37–42 °C, except for the thermostable AsCas12a, AapCas12b, and BrCas12b which can work up to 70 °C.[35–37]

To elucidate the fundamental working principles of the class 2 nucleases, we select class 2 representative proteins including spCas9, catalytically inactivate spCas9 (dCas9), LbCas12a, and LwCas13a to explain their working mechanisms for the nucleic acid-targeting diagnostics in Fig. 1.

The spCas9 variant isolated from *Streptococcus pyogenes* was the first CRISPR system discovered to be programmable and engineered for sequence cleavage.[11] The Cas9 ternary as shown in Fig. 1a consists of Cas9 protein, programmable sgRNA, and target sequence. The DNase activity of Cas9 is directed by a dual crRNA-*trans*-activating CRISPR RNA (tracrRNA) complex to break the target dsDNA at specific loci near the PAM, where the chimeric sgRNA is fused by the crRNA and tracrRNA. After the programmable sgRNA spacer binds to the target protospacer sequence, the HNH and RuvC nuclease domains of the enzyme are activated to cleave both the targeting and non-targeting sequences, respectively (Fig. 1a). In addition, Cas9 can be guided to cleave ssRNA with the presence of PAM-presenting oligonucleotides (PAMmers).[38] Recently, it was found that in the case of the Cas9 derived

Table 1 Characteristics of class 2 CRISPR–Cas systems for molecular diagnostics

Type	Variant	Origin	Target	Spacer length	PAM/FPS (5′ to 3′)	Cleavage loci	Sensitivity	Ref.
Cas9	spCas9	*Streptococcus pyogenes*	dsDNA	20	NGG	4th	—	11
Cas12	Lbcas12a	*Lachnospiraceae bacterium*	ssDNA, dsDNA	22	TTTV	22nd	41.5 pM	45
	Ascas12a	*Acidaminococcus* sp.	ssDNA, dsDNA	20	TTTV	24th	50 nM	46, 47
	AacCas12b	*Alicyclobacillus acidoterrestris*	ssDNA, dsDNA	20	TTTV	24th	—	37, 48
	BhCas12b	*Bacillus hisashii*	ssDNA, dsDNA	22	TTN	—	—	49
	AapCas12b	*Alicyclobacillus acidiphilus*	dsDNA	20	TTN	23rd	1.6 nM (ssDNA) 8 nM (dsDNA)	50, 51
	Un1Cas12f1 (Cas14)	Uncultivated archaea	ssDNA	20	NA	23rd	—	52
	Un1Cas12f1 (Cas14)	Uncultivated archaea	dsDNA	20	TTTA	20–24 bp	—	53
Cas13	LshCas13a	*Leptotrichia shahii*	RNA	28	FPS, H	Multiple	—	54
	LwaCas13a	*Leptotrichia wadei*	RNA	28	NA	Multiple	50 pM	46
	LbuCas13a	*Leptotrichia buccalis*	RNA	20	NA	Multiple	10 fM	18, 55
	LbaCas13a	*L. bacterium* NK4A179	RNA	28	NA	Multiple	1 nM	46
	CcaCas13b	*C. canimorsus*	RNA	30	NA	Multiple	50 pM	46
	PsmCas13b	P. sp. A2016	RNA	30	NA	Multiple	5 nM	46

from *Campylobacter jejuni*, the tracrRNA hybridizes to cellular RNAs which leads to the formation of "noncanonical" crRNAs capable of guiding DNA targeting by Cas9, where the guided RNA is unassociated with viral defence.[39] This discovery inspired the reprograming of tracrRNA that can be linked to the presence of any RNA of interest for DNA cutting. Therefore, this method expands the programmable designs of the Cas9 system within the dual RNAs complex from the conventional crRNA spacer region to tracrRNA.

After mapping the locations of both HNH and RuvC nuclease domains, either of these two nuclease domains can be silenced by point mutation to create a programmable Cas9 nickase (Cas9n) that generates a nick at the targeted sequence. Furthermore, spCas9 can be switched to catalytically inactive Cas9 (dCas9) without any nuclease activities.[40] As shown in Fig. 1b, the dCas9 possesses the same Cas9 ternary including dCas9, sgRNA, and target sequence. This feature allows the dCas9 system

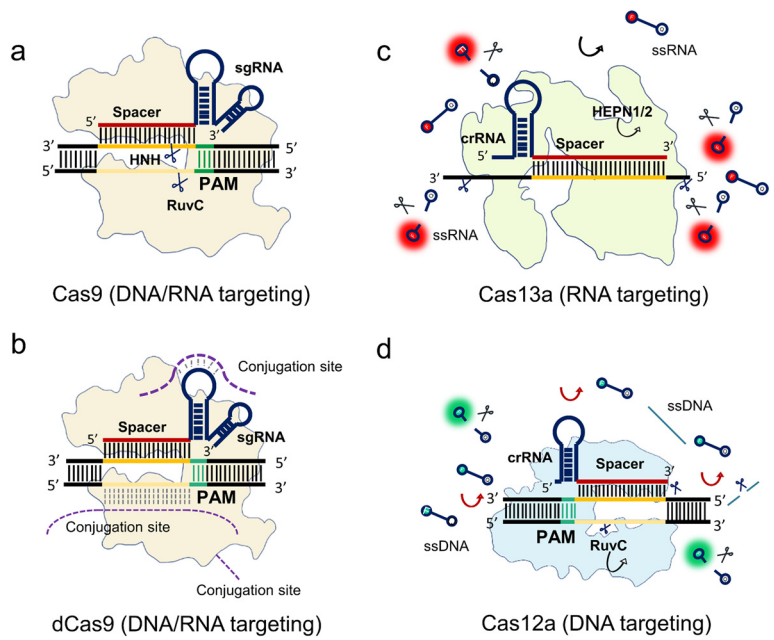

Fig. 1 Mechanisms of class 2 CRISPR–Cas systems. (a) Cas9 with a sgRNA binds to a target dsDNA. The HNH and RuvC nuclease domains cleave the corresponding strands near the PAM. (b) The dCas9 system is a nuclease inactive Cas9 system. The sgRNA-guided dCas9 protein binds to the target sequence without any sequence break. The external functions of the dCas9 system can be conjugated from the sgRNA stem-loop sequence, non-target sequence, and dCas9 protein. (c) The crRNA-guided Cas13a binds to a target RNA enabling *trans*-cleavage of surrounding ssRNAs. (d) The crRNA-guided LbCas12a binds to a target DNA near the PAM enabling *trans*-cleavage of surrounding ssDNA. All the programmable spacers of the class 2 RNA sequences are annotated in red, while the target sequence and non-target sequence are denoted as deep and light orange, respectively. The PAM sequences are in green.

to recognize any sites in the genome near the PAM, similar to the function of antibody and antigen conjugation. To extend this powerful labeling ability, extended functions of the dCas9 system are developed *via* conjugations from different sites (Fig. 1b). Oligonucleotide probes with different tags such as nanoparticles and fluorophores can be conjugated at the nucleic acid stem-loop and non-target sequence sites. Comparably, the dCas9 protein is another conjugation site for other functional proteins and oligonucleotide probes.

Cas9 guided by sgRNA only cleaves the target strand within the spacer region. In contrast, Cas13 has been reported as an RNA-guided RNA targeting system that not only cleaves the target strand but also the surrounding RNAs. This RNase activity of *trans*-cleaving the surrounding ssRNAs is named collateral activity or *trans*-cleavage (Fig. 1c).[17] Specifically, the crRNA guides LwCas13a to detect the target RNA. LwCas13a can *trans*-cleave the surrounding ssRNA, after binding to the target RNA.[17,18,41,42] Unlike the Cas9 family, most reported variants of the Cas13 family have no PAM requirements except for LshCas13a from *Leptotrichia shahii*, which can be constrained by a sequence constraint termed PFS restriction where no G base is required.[17]

Similar to the Cas13 system, the Cas12a family has a *trans*-cleavage ability of ssDNA.[43,44] As shown in Fig. 1d, LbCas12a is guided by its crRNA to target the dsDNA sequence near the PAM. After binding to the target sequence, Cas12a cleaves both the targeting strand and the non-targeting strand at a specific position. At the same time, the *trans*-cleavage ability is activated to cleave the surrounding ssDNA. Most of the Cas12 family has PAM sequence constraints like Cas9.

In summary, the mechanisms of CRISPR-based detection can be broadly classified into two categories, non-collateral cleavages (Cas9 and dCas9) and collateral cleavages (Cas12 and Cas13). For the non-collateral detection methods, Cas9 is a programmable endonuclease. In addition, dCas9, in which the sequence nicking ability is muted, can be utilized for specific bio-recognition, or target enrichment *via* different links including the sgRNA, protospacer, and protein conjugation. Comparably, the collateral effect of Cas12 and Cas13 harnesses the *trans*-cleavage ability for enhanced bio-reporting. Thus, some of these Cas enzymes exhibit high sensitivity, ranging from femtomolar to picomolar, allowing amplification-free detection in certain scenarios.

3 Isothermal amplification-assisted detection

3.1. Isothermal amplification schemes in CRISPR systems

The CRISPR-based diagnostic tool is programmable and specific, but its sensitivity would be still limited to the picomolar level without any amplification. For ultrasensitive detection, preamplification is required for increasing the limit of detection (LOD). Among the nucleic acid amplification schemes, isothermal alternatives require less complicated setups compared to PCR thermal cycling, which is promising for meeting the ASSURED standard. The isothermal assays, including loop-mediated isothermal amplification (LAMP),[56] recombinase polymerase amplification (RPA),[57] strand displacement amplification (SDA),[58] nucleic acid sequence-based amplification (NASBA),[59] exponential amplification reaction (EXPAR),[60] and rolling circle amplification (RCA),[61] have all been demonstrated in combination with CRISPR assays (Table 2). More recently, some of these methods were developed to combat the SARS-CoV-2 pandemic in different formats.[62–69] Compared to the gold standard PCR which has a $\sim 10^9$ amplification efficiency and SNP detection ability,[70] isothermal methods such as HRCA, LAMP, and RPA have shown equal amplification efficiency to PCR, while NASBA and EXPAR are less efficient. Overall, isothermal amplification methods tend to generate non-specific results because of their relatively lower annealing temperature. Augmentation of those assays always requires additional special designs (*e.g.*, probes, and exonuclease) to enhance specificity.[71–73] Therefore, the recent integrated methods of isothermal amplification and CRISPR detection have shown unprecedented specificity at extremely low concentrations (*e.g.*, down to the attomolar level), where the signals are only triggered in the presence of the target objects.

The selection of the nucleic acid amplification scheme is largely dependent on the type of target and CRISPR effectors. DNA and RNA targets can be commonly amplified by RPA, LAMP, or NASBA, while SDA, EXPAR, and RCA are more frequently applied to miRNAs because the length of miRNAs restricts the primer design.[70] When it comes to the influence of CRISPR effectors, non-collateral detection of Cas9 requires additional design for signal reporting, which would significantly affect the options of the amplification methods. In comparison, the final activators of Cas12 and Cas13 for

Table 2 Isothermal amplification schemes used in CRISPR assays

Method	Enzymes	No. of primers	Temperature (°C)	Reaction time (min)	Efficiency	Ref.
NASBA	Reverse transcriptase and RNA polymerase (RNase H)	2	~41	90–120	10^6–10^9	59, 74
E-SDA	DNA polymerase and NEase	2 or 4	37	120	10^7	58, 75
HRCA	Ligase and DNA polymerase	2	37	90	10^9	61, 76
LAMP	DNA polymerase	4 or 6	60–65	30–60	10^9	56, 77
RPA	DNA polymerase and recombinase	2	37–42	10–30	10^9	57
EXPAR	DNA polymerase and NEase	0	50–60	30	10^6–10^8	60, 78

Table 3 Isothermal amplification assisted diagnostics with Cas9

Variant	Name	Amplification methods	Time (min)	Target	LOD (aM)	LOD (cp mL^{-1})	Visualization methods	Ref.
spCas9	NASBACC	NASBA	180	RNA	1×10^3	6×10^5	Fluorescence	12
spCas9	CAS-EXPAR	EXPAR	60	DNA	0.82	4.9×10^2	Fluorescence	80
spCas9	CRISDA	SDA	190	DNA	6.7	4×10^3	Fluorescence	79
dCas9		RPA	20	DNA RNA	0.54	3×10^2	Silicon microring resonator	90
dcas9	RCH	RCA	240	miRNA	35.4	2.1×10^4	Colorimetry	87
spCas9	Cas9nAR	Nickase-based amplification reaction	60	DNA	0.167	1×10^2	Fluorescence	82
spCas9	RACE	RCA	240	microRNA	9×10^4	5.4×10^7	Fluorescence	91
spCas9	CUT-LAMP	LAMP	60	DNA	5	3×10^6	Fluorescence	92
spCas9	CASLFA	RPA	60	DNA	12.5	7.5×10^3	LFA	85
spCas9		Nickase-triggered amplification	80	DNA	16	9.6×10^3	LFA	83
spCas9		SDA–RCA	150	DNA	1.87×10^3	1.1×10^6	Fluorescence	93
dCas9		RT-RPA	37	RNA	6.7	4×10^3	LFA	86
spCas9		SDA	65	DNA	1.3×10^7	7.8×10^9	Electrochemical	94
FnCas9	FELUDA	RPA	60	RNA	33	2×10^3	LFA	95
dCas9	Vigilant	RPA	35	RNA	4.2	2.5×10^3	LFA	96
dCas9	Bio-SCAN	RPA	24	RNA	6.67	4×10^3	LFA	89
dCas9		RPA–RCA	—	DNA	20	1.2×10^4	LFA	97
spCas9	Cas9 nAR-v2	SDA	60	RNA	0.83	5×10^2	Fluorescence/LFA	98
spCas9	DAMPR	LAMP	50	RNA	~1	6×10^2	Fluorescence	99

collateral cleavage are DNAs and RNAs, respectively. Since most of the amplification methods would generate DNA amplicons using DNA polymerase, the specific design of T7 transcription is required to produce RNA amplicons. Therefore, the Cas12 family can be easily integrated with most of these methods. In contrast, the Cas13 family requires an extra T7 transcription step to generate RNA activators. To date, RPA and LAMP are regarded as the most popular candidates to be integrated with CRISPR owing to their fast reaction and high amplification efficiency.

3.2. Cas9 detection systems with isothermal amplification

Cas9 is a powerful CRISPR tool that can be used as a programmable endonuclease for specific sequence cleavage with switchable nuclease activities. In addition to the nuclease function, the engineered dCas9 with different conjugations has been applied to molecular diagnostics, *in situ* nucleic acid imaging, *etc.* In this section, we summarize the strategies using Cas9 for diagnostics in different scenarios.

Table 4 Isothermal amplification assisted diagnostics with Cas13

Variant	Name	Amplification methods	Time (min)	Target	LOD (aM)	LOD (cp mL^{-1})	Visualization	Ref.
Lwcas13a	SHERLOCK	RPA	60	NA	2	1×10^3	Fluorescence	41
Lwcas13a, LbCas13b, Ascas12a	SHERLOCKv2	RPA	60	NA	8×10^{-3}	4.8	Fluorescence LFA	46
Lwcas13a	HUDSON–SHERLOCK	RPA	60	RNA	2	1×10^3	Fluorescence LFA	100
Lwcas13a		RPA	46	NA	16.7	1×10^4	Colorimetric	115
LbuCas13a	DISCoVER	LAMP	35	RNA	16.7	1×10^4	Fluorescence	109
Lwcas13a	CARMEN–Cas13	RPA	60	NA	2	1×10^3	Digital fluorescence (multiplexed)	104
Lwcas13a		RPA	105	DNA	0.6	4×10^2	LFA	116
LwCas13a		RPA	60	RNA	1.4	8.4×10^2	LFA/fluorescence	117
Lwcas13a		RPA	60	RNA	16.7	1×10^4	LFA/fluorescence	101
LwCas13a	SHINE	RPA	40	RNA	16.7	1×10^4	LFA	102
LwCas13a	MEDICA	RPA	25	DNA	2	1×10^3	Digital fluorescence	108
LwCas13a	PADLOCK	RPA	30	DNA	2	1×10^3	Digital fluorescence	73
LbuCas13a		RCA	120	miRNA	5×10^2	3×10^6	Fluorescence	111
LwCas13a	SHINEv2	RPA	90	RNA	1.7×10^2	1×10^6	LFA (POCT)	118
LwCas13a PsmCas13b		RPA	60	RNA	0.3	1.8×10^2	Fluorescence (multiplexed)	119
LwCas13a	ADESSO	RPA	60	RNA	4.2	2.5×10^3	Fluorescence	120
TccCas13a	OPTIMA-dx	LAMP	45	RNA	16.7	1×10^4	Fluorescence	121

Table 5 Isothermal amplification assisted diagnostics with Cas12

Variant	Name	Amplification methods	Time (min)	Target	LOD (aM)	LOD (cp mL^{-1})	Visualization methods	Ref.
LbCas12a	DETECTR	RPA	70	DNA	2	1×10^3	Fluorescence	44
LbCas12a	ULC	LAMP	45	DNA	16.7	1×10^4	Fluorescence	139
AacCas12b	HOLMESv2	LAMP	60	NA	10	6×10^3	Fluorescence	37
LbCas12a	Cas12a-SCR	RCT	420	miRNA	1.7×10^5	1×10^8	Fluorescence	135
LbCas12a		RPA	75	DNA	16.7	1×10^4	Fluorescence	140
LbCas12a	CIA	LAMP	50	DNA	1	6×10^2	LFA	141
LbCas12a		LAMP	40	RNA	1.3	7.8×10^2	Fluorescence	142
LbCas12a		LAMP	35	DNA	—	—	Colorimetry	143
LbCas12a	SHERLOCK-Cas12a	RPA	60	DNA RNA	50	3×10^4	LFA	144
LbCas12a		LAMP	160	DNA	10	6×10^3	Colorimetry	145
LbCas12a		HRCA	420	miRNA	2×10^3	1×10^6	Fluorescence	136
LbCas12a		LAMP	40	RNA	2	1×10^3	LFA	129
LbCas12a		LAMP–RPA	60	RNA	0.1	60	LFA	47
LbCas12a	AIOD-CRISPR	RPA	40	RNA	0.33	2×10^2	Fluorescence	122
AapCas12b	STOP	LAMP	45	RNA	0.055	3.3×10^1	Fluorescence	50
AsCas12a	CIRI	RCA	—	DNA	1	6×10^2	Optomagnetic	134
LbCas12a	ITP–CRISPR	LAMP	35	RNA	16.7	1×10^4	Fluorescence	130
LbCas12a	CIALFB	LAMP	50	DNA	3.1	1.8×10^3	LFA	146
LbCas12a		LAMP	60	DNA	—	—	Fluorescence	147
LbCas12a		LAMP	40	RNA	50	3×10^4	Fluorescence	148
LbCas12a AacCas12b AapCas12b	iSCAN	LAMP	60	RNA	0.33	2×10^2	Fluorescence	149
LbCas12a		RPA	30	RNA	3.3×10^{-2}	20	Surface plasmon resonance colorimetric	150
LbCas12a	MCDC	RPA	55	RNA	1.67	1×10^3	Colorimetry	151
LbCas12a		LAMP	40	DNA	800 CFU ml^{-1}	—	Fluorescence	152
LbCas12a	opvCRISPR	LAMP	45	RNA	0.21	1.3×10^2	Fluorescence	153
LbCas12a		RPA	40	RNA	0.63	3.8×10^2	Fluorescence	113
LbCas12a	WS-CRISPR	LAMP	90	RNA	83.3	5×10^4	Digital fluorescence	133
LbCas12a		LAMP	60	DNA	1.67	1×10^3	Fluorescence–LFA	154
LbCas12a	DECOVID	RPA	30	RNA	1.67	1×10^3	Digital fluorescence	126
LbCas12a	RADICA	RPA	60	DNA	1.5	9×10^2	Digital fluorescence	155
AsCas12a	VaNGuard	LAMP	52	RNA	3.33	2×10^3	Fluorescence LFA	156
Lbcas12a	CAL-LAMP	LAMP	—	miRNA	1×10^4	6×10^5	Fluorescence	157
LbCas12a	CLAP	LAMP	40	RNA	6.67	4×10^3	Colorimetry	158
LbCas12a		RPA	60	RNA	6.67	4×10^3	Fluorescence (POCT)	159
LbCas12a	POC-CRISPR	RPA	60	RNA	1 GE μL^{-1}		Fluorescence (POCT)	160
Aapcas12b	WS-RADICA	LAMP	60	RNA	2	1.2×10^3	Digital fluorescence	161
BrCas12b		LAMP	30	RNA	10	6×10^3	Fluorescence	132
LbCas12a	sPAMC	RPA	20	RNA	2	1.2×10^3	Fluorescence	123
LbCas12a		LAMP	45–75	RNA	166.7	1×10^5	Fluorescence	162
LbCas12a		RPA	40	DNA	0.16	96	Fluorescence	163
LbCas12a	DropCRISPR	LAMP	>60	DNA	102 cfu mL^{-1}	—	Fluorescence	164
LbCas12a	FAST	RPA	50	RNA	1×10^4	6×10^6	Fluorescence	165
AsCas12a	UCAD	RPA	>40	Antibodies	10	6×10^4	Fluorescence	166
LbCas12a	MiCaR	RPA	40	DNA	0.26	1.6×10^2	Fluorescence (multiplexed)	167
LbCas12a		RPA	30	RNA	1.67	1×10^3	Fluorescence	168
LbCas12a	MAPnavi	RPA	40	RNA	0.33	2×10^2	Fluorescence	169

3.2.1. Endonuclease activity of Cas9. The first combination of CRISPR–Cas9 and nucleic acid detection was introduced by Collins *et al.*[12] termed NASBA-CRISPR cleavage (NASBACC), whereby they designed the NASBA-based preamplification scheme for RNA detection (Fig. 2a). They combined a synthetic toehold sensor with a Cas9 system for the specific SNP typing. This whole process contains RNA NASBA preamplification, Cas9 selective cleavage, T7 full-length RNA transcription, and toehold sensor activation. Because toehold detection needs RNA of at least 30 nM to trigger a visible reaction, the NASBA preamplification is significant for amplifying the target object of interest first. After the target amplification, the Cas9 ribonucleoprotein was applied to differentiate the SNP difference located in the PAM sequence before RNA transcription. Generally, in the presence of appropriate PAM, the Cas9 guided by sgRNA cleaves the amplicons to produce truncated RNA products that are unable to activate the toehold sensor. Comparably, a mutation in PAM prevents Cas9 from breaking the strand, resulting in full-length RNA transcription. This full-length transcribed

Table 6 Summary of amplification-free CRISPR detection methods

Type	Variant	Name	Time (min)	Target	LOD (aM)	LOD (cp mL^{-1})	Visualization	Ref.
Cas9	dcas9	CRISPR DNA-FISH	30	DNA	10 cfu ml^{-1}		Fluorescence	180
	dcas9	Paired dCas9 (PC) reporter	30	DNA	5×10^4	3×10^7	Luminescence	201
	dcas9		30	DNA	—	—	Colorimetry	202
	dcas9	CRISPR chip	15	DNA	1.7×10^3	1×10^6	FET-electricity	176
	dcas9		90	RNA	1.4×10^8	8.4×10^{10}	Colorimetry	203
	dcas9	CRISPR-SERS	60	DNA	8.1×10^3	4.8×10^6	Surface-enhanced Raman	181
	dcas9	CRISPR-SNP-Chip	60	DNA	—	—	FET-electricity	182
	dCas9		60	DNA	3×10^2	1.8×10^5	LFA	187
Cas12	Lbcas12a	E-CRISPR	40	DNA	5×10^7	3×10^{10}	Electrochemical	183
	Lbcas12a	IMPACT	120	DNA	1×10^8	6×10^{10}	Fluorescence	204
	LbCas12a	E-DNA	30	DNA	1×10^4	6×10^6	Electrochemical	205
	Lbcas12a		1440	DNA	1×10^4	6×10^6	Fluorescence	206
	Ascas12a		20	DNA	1×10^5	1×10^7	Electrochemical	186
	Lbcas12a	CONAN	30	DNA	5	3×10^2	Fluorescence	175
	LbCas12a	CSMBA	10	DNA	3	1.8×10^3	Fluorescence	207
	LbCas12a		30	DNA	1×10^6	6×10^8	Fluorescence (tandem crRNA)	208
	LbCas12a		5	miRNA	1×10^4	6×10^6	Fluorescence (gold nanoparticles)	209
	LbCas12a LwCas13a		>30	DNA RNA	16.67	1×10^4	Quantum dot-based molecular beacons	210
	LbCas12a	MOPCS	38	RNA	1.5×10^4	9×10^6	Plasmon resonance	211
Cas13	LbuCas13a		30	RNA	1×10^6	6×10^8	Fluorescence	18
	LbuCas13a		30	miRNA	4.5×10^5	2.7×10^8	Fluorescence	110
	LwCas13a		5	RNA	9×10^4	5.4×10^7	Fluorescence	212
	LwCas13a		240	miRNA	1×10^7	6×10^9	Electrochemical	194
	LbuCas13a	CLISA	300	Protein	8.1×10^3	4.8×10^6	Fluorescence	213
	LbuCas13a	PECL-CRISPR	70	miRNA	1×10^3	6×10^5	Electricity	195
	LwCas13a	CRISPR-Biosensor X	180	miRNA	2×10^6	1.2×10^9	Electrochemical	196
	LwaCas13a	CRISPR-FET	20	RNA	1.56	9.4×10^2	FET-electricity	214
	LbuCas13a	SHARK	90	RNA	1×10^4	6×10^6	LFA/digital bioluminescence	215
	LwaCas13a	CRISPR Cas13agFET biosensor	30	RNA	1	6×10^2	gFET-electricity	177
	LtrCas13a	opn-SATORI	9	RNA	6.5	3.9×10^3	Digital fluorescence	216
	LbuCas13a LwaCas13a	CrisprZyme	270	RNA	8.3×10^4	5×10^7	Colorimetric	217
	LwaCas13a		30	RNA	1	6×10^2	Electrochemical	218

RNA activates the toehold sensor for colorimetric readout. Therefore, this Cas9-based toehold detection method can achieve SNP detection ability to differentiate the Zika (*e.g.*, African Zika and American Zika) virus down to 2.8 fM.

3.2.2. Nicking endonuclease ability of Cas9. In addition to sequence cleavage, Cas9 can also be engineered as a programmable nickase that can selectively cut target strands as desired by silencing either nuclease domain of Cas9 through point mutations. To achieve the sequence nicking instead of digestion, the high specificity of Cas9 with a mutation of the HNH catalytic residue was leveraged to combine with E-SDA. This method named the CRISPR–Cas9-triggered nicking endonuclease-mediated SDA method (CRISDA) achieved attomolar sensitivity and SNP specificity (Fig. 2b).[79] First, the sgRNA-guided Cas9 was introduced to nick the target strand, where the SDA primer was bound to the exposed sequence to trigger SDA amplification. After amplification, the biotin-labeled peptide nucleic acid (PNA) and Cy5-labelled PNA probes targeting the central region of the amplicon were added to quantitatively determine the target DNA amplified by the fluorescence intensity of Cy5 after a simple magnetic pull-down by streptavidin-labeled magnetic beads. The original SDA method relies on an extra denaturation step to unwind dsDNA, limiting its practical applications for DNA detection.[58,75] The CRISDA method utilizes the engineered Cas9 to select the target object sequence of interest and expose the initial binding sites, which not only improves the specificity but also eliminates the denaturation step.

A similar design of EXPAR in combination with Cas9 was used for mRNA detection.[80] Since EXPAR is widely adopted for short nucleic acid detection such as microRNAs,[81] the desired RNA sequence is cut off by Cas9 directed by a sgRNA in the presence of the PAMmer. Subsequently, the cleaved fragments hybridize with the EXPAR template and are amplified accordingly. This method can detect any sites of single-strand targets by the programmable sgRNA with the sequence selection of the Cas9 and EXPAR system.

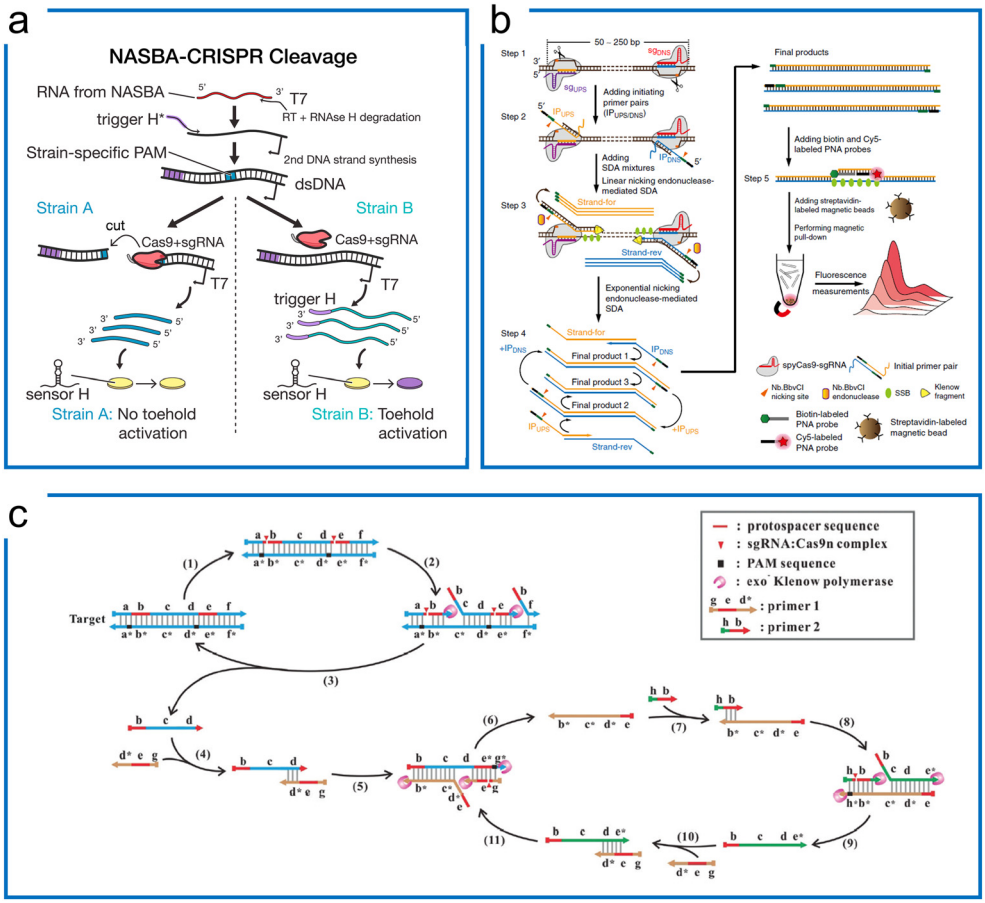

Fig. 2 Isothermal amplification enhanced Cas9 nucleic acid detection. (a) The Zika virus detection with Cas9 for SNP visualization. The target RNA was firstly amplified by NASBA, followed by the Cas9 cleavage to differentiate the SNP difference due to the PAM requirement. Finally, the synthetic biology of the toehold sensor enables colorimetric visualization. The figure was reproduced from ref. 12 with permission from Elsevier, copyright 2016. (b) The CRISDA method uses SDA and Cas9, where programmable cas9n nicks the binding region for SDA primer binding and amplification. The amplicons were visualized by additional fluorescence. The figure was reproduced from ref. 79 under Creative Commons Attribution License from Springer Nature, copyright 2018. (c) The Cas9nAR design for universal dsDNA detection includes primers, DNA polymerase, and sgRNA/Cas9n complex. The Cas9n serves as the programmable nicking enzyme in the SDA. The figure was reproduced from ref. 82 with permission from John Wiley and Sons, copyright 2019.

However, even though CRISPR–Cas9 can be applied to specifically cut off the target sequence, these two aforementioned methods still rely on extra nicking endonucleases in their design even though Cas9 already has a nicking ability. The Cas9 nickase-based amplification reaction (Cas9nAR) was developed for genomic DNA upon the precise recognition ability of the target object site (Fig. 2c),[82] whereby the 11-step reaction in a one-pot assay can be designed as a universal method containing cycles of DNA replication through priming, extension, nicking, and displacement reaction steps. This method harnesses an sgRNA : Cas9n complex with a single-strand nicking property, a strand displacing DNA polymerase, and two primers bearing the cleavage sequence of Cas9n. The Cas9 ribonucleoprotein has been utilized for selecting the target of interest from the raw genomic DNA as well as for SDA amplification as the nicking enzymes. This one-pot reaction has achieved 0.1 copies per μL sensitivity within 60 min, highlighting the potential applications of Cas9-based SDA methods for universal detection. With the lateral flow assay (LFA) visualization introduced later, this method achieved 16.7 aM sensitivity in detecting food-borne pathogens.[83] However, this approach is challenging to implement due to the constraint of the two PAM sequence designs.

3.2.3. Single-strand probe binding to the stem-loop of dCas9 sgRNA. Compared to Cas9, which is applied for sequence nicking or digestion, dCas9 attains the equivalent sensitivity and specificity as Cas9 despite the muted nuclease activities. Li *et al.*[84] designed a detection method for single nucleotide variant (SNV) of the ND4 and ND5 genes in the mitochondrial DNA (mtDNA) using two dCas9 systems for the proximity ligation assay (Fig. 3a). Base pairs of sgRNA to the protospacer are sensitive to the presence of a mutation. Hence, the dCas9 ribonucleoprotein can differentiate the SNVs when binding to the mtDNA. A pair of sgRNAs were designed to recognize the sequence that is nearby within the genome. When the two dCas9 ternaries were close to each other, two linear DNA oligonucleotides base pairing to the

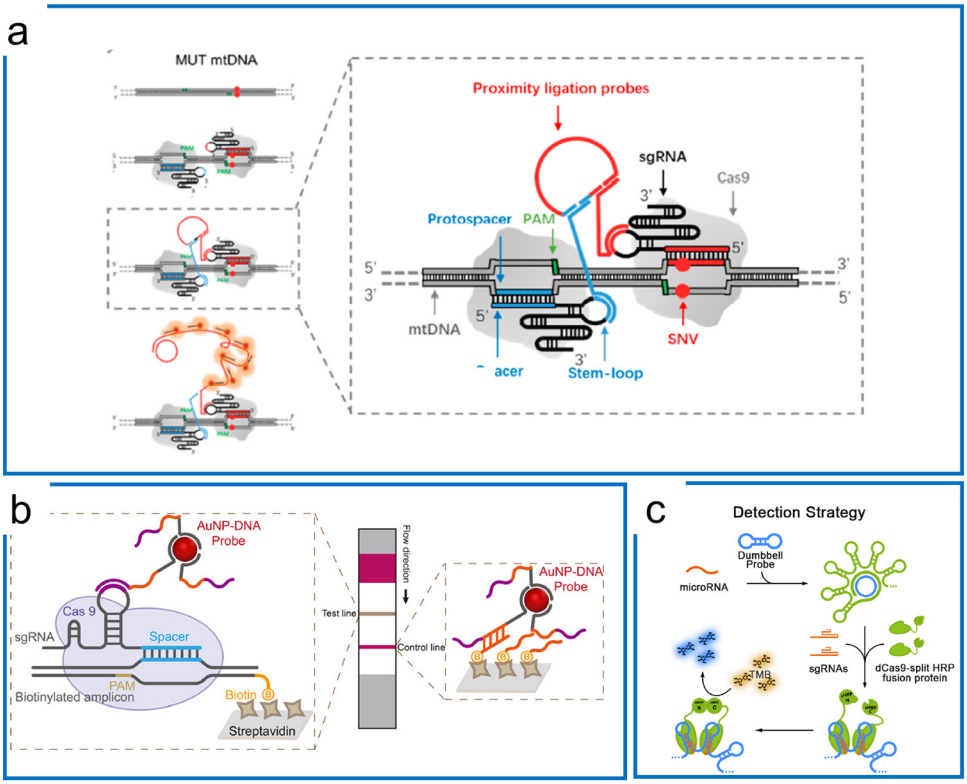

Fig. 3 Isothermal amplification assisted dCas9 molecular diagnosis. (a) The dCas9 system with a proximity ligation assay coupled with RCA for SNV detection. The two Cas9 ribonucleoproteins differentiate the mutations of the sequence in the protospacer region. The *in situ* difference is visualized by the proximity ligation assay using two DNA probes binding to stem-loops of these two sgRNAs. Adapted from ref. 84. Copyright 2018 American Chemical Society. (b) The dCas9-based detection using AuNPs–DNA probes hybridizing to either the stem-loop of sgRNA or non-targeting sequence. The RPA preamplification tags the biotin for hybridization with the streptavidin on the surface of the LFA strip. Adapted from ref. 85. Copyright 2020 American Chemical Society. (c) The microRNA detection using dCas9-splint HRP fusion protein for colorimetric readout. The dumbbell amplicons are synthesized by RCA amplification using microRNA and padlock probe ligation. After dCas9 systems are bound to the dsDNA region of the amplicons, the TMB is introduced to react with HRP for colorimetric readout. Adapted from ref. 87. Copyright 2018 American Chemical Society.

two stem-loops of sgRNA directed the ligation of a circulated template for rolling circle amplification. Thus, the rolling circle amplification results were converted into the visualization of mutations on the mtDNA at a single base resolution. This work established a method to study SNP *in situ* in single cells with dCas9.

3.2.4. Single-strand probe binding to the non-targeting sequence of the protospacer. The conventional LFA assay uses the tagged primers to amplify the target sequence. The dual-labeled amplicons can bind to the precoated affinity ligand or gold-based probes on the paper substrate *via* capillary force for capture and visualization. Zhou *et al.* designed a dCas9-based method for LFA readout (Fig. 3b). This method utilized the dCas9 for target sequence labeling. After the dCas9 ribonucleoprotein bound to the target sequence, the non-targeted sequence and stem-loop of sgRNA were adopted for gold nanoparticle (AuNP)–DNA probe conjugation. Here, the biotin-modified primers at the 5 end were utilized for the isothermal pre-amplification. The biotin-introduced amplicons were immobilized on the streptavidin-coated paper surface, where the dCas9 ribonucleoprotein bound to the target amplicons specifically, and the AuNP–DNA probes were then hybridized to either the stem-loop or non-targeting sequence, which was followed by a washing step for visualization.[85] By designing two detection regions, this work was further adopted for SARS-Cov-2 detection with stem-loop hybridization.[86]

3.2.5. Direct conjugation to dCas9. Other than the base pairing to the exposed single-strand *via* covalent bonding, the dCas9 protein has been linked to split horseradish peroxidase (split-HRP) for colorimetric readout using chimeric fusion. In this design, a dumbbell padlock probe was used to detect microRNA *via* ligation.[87] The circulated padlock probe enabled a rolling circle amplification to generate dsDNA sequences, which could be recognized by the modified dCas9 systems (Fig. 3c). The dCas9 protein was pre-fused with the split-HRP report fragment. The split-HRP–dCas9 fusion protein guided by sgRNA was recruited around a scaffold-like structure of RCA products to perform HRP activity, where tetramethylbenzidine (TMB) was introduced for a colorimetric readout. A similar idea of chimeric fusion between dCas9 and VirD2 relaxase was developed by Mahfouz *et al.*[88] The chimeric fusion between a CRISPR enzyme and a relaxase can provide the dual functions of specific binding to the target sequence through dCas9 and binding to a FAM-tagged ssDNA probe *via* VirD2, resulting in a molecular complex for LFA

detection. This group later employed dCas9 biotinylation to form the biotin-labeled dCas9 and sgRNA complex to realize the same diagnosis purpose with the LFA assay.[89]

3.3. Cas13 detection systems with isothermal amplification

The significant difference between Cas9 and Cas13 is that Cas13 is an RNA targeting system with both *cis* and *trans*-cleavage ability. Therefore, the nucleic acid diagnostics with the Cas13a system utilize the specific *cis* targeting ability of the Cas13 system to enable *trans*-cleavage of engineered ssRNAs (*e.g.*, ssRNA probes). To achieve a comparable LOD as PCR, the Cas13-based diagnostics involve preamplification and Cas13 detection including T7 transcription and Cas13 visualization. Here, we summarize the representative Cas13 systems according to the different isothermal amplification methods.

3.3.1. RPA-based Cas13 assays. LwCas13a is the first CRISPR enzyme to be applied to nucleic acid detection integrated with isothermal preamplification. The first LwCas13a-based method was developed and named Specific High-Sensitivity Enzymatic Reporter UnLOCKing (SHERLOCK). This method achieved 2 aM sensitivity within an hour. The SHERLOCK assay could detect both RNA and DNA through the RT-RPA or RPA preamplification, T7 transcription, and *trans*-cleavage of ssRNA reporters (Fig. 4a).[41] The later discovery of di-nucleotide preferences of different species of the type V family has led to a multiplexed ability with the collateral activity of 4 channels (PsmCas13b, LwaCas13a, CcaCas13b, and AsCas12a) (Fig. 4b).[46]

Subsequently, the SHERLOCK assay was coupled with the HUDSON (unextracted author manuscript diagnostic samples to obliterate nucleases) protocol to detect the Zika virus and dengue fever virus in patient samples with the LOD of a single copy per microliter (Fig. 5a).[100] This protocol was then further applied to detect Ebola and SARS-CoV-2.[101,102] Recently, machine learning was applied to simplify the sequence design process and optimize the primers and crRNA of the SHERLOCK assay.[103] The SHERLOCK assay has been combined with droplet array technology to realize massively multiplexed pathogen detection. This method is termed combinatorial arrayed reactions for multiplexed evaluation of nucleic acids with Cas13 (CARMEN–Cas13) (Fig. 5b).[104] The high multiplexable ability was achieved by the preparation of the color code droplets of 4 fluorescent colors with different concentrations individually to make 1050 color codes.[105] Each RPA preamplified sample or Cas13a detection mix was emulsified into droplets with a distinct color code. All droplets were pooled and loaded on a microarray chip where the droplets self-organized into pairs and the positions of each sample and crRNA were identified by their color codes. The droplet pairs were then merged for the initiation of CRISPR assays to obtain the positive detection results. Later, Myhrvold *et al.* upgraded the CARMEN with Fluidigm microfluidics to reduce the operation time.[106] This isothermal massive detection has the advantage of decreasing reagent costs per test by more than 300 times compared to the conventional bulk reaction. Quantitative measurement is of great importance for biological studies, and in order to increase the accuracy of quantification and reduce false-positive events, a microfluidic-enabled digital isothermal Cas13a assay (termed MEDICA) has been developed (Fig. 5c). In traditional setups,

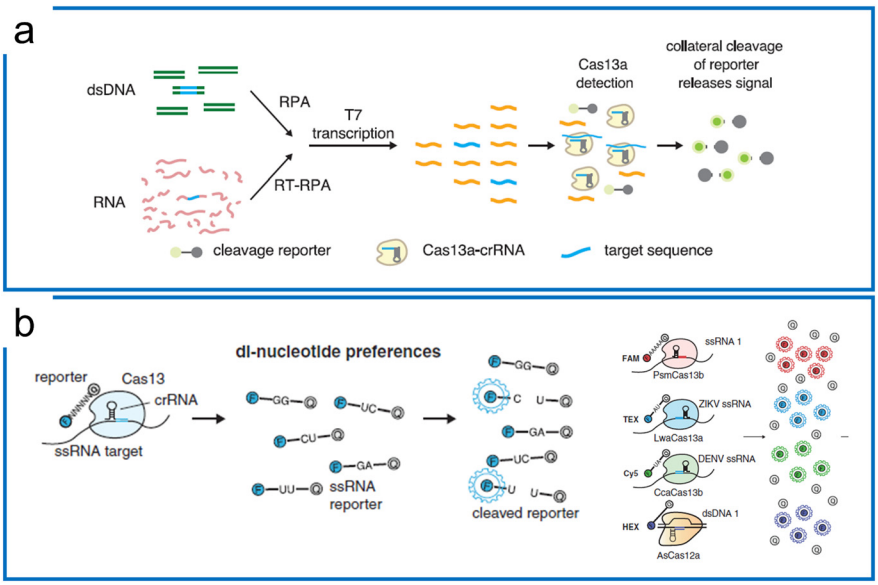

Fig. 4 Theory of Cas13-based diagnostics. (a) SHERLOCK nucleic acid detection platform includes RPA preamplification, T7 transcription, and Cas13a detection. The figure was reproduced from ref. 41 with permission from the American Association for the Advancement of Science, copyright 2017. (b) The di-nucleotide preferences of the Cas13 family and AsCas12a combination enable 4 channel multiplexed diagnostics with different fluorescence probes including ssRNA probes (Cas13 family) and ssDNA probe (Cas12). The figure was reproduced from ref. 46 with permission from the American Association for the Advancement of Science, copyright 2018.

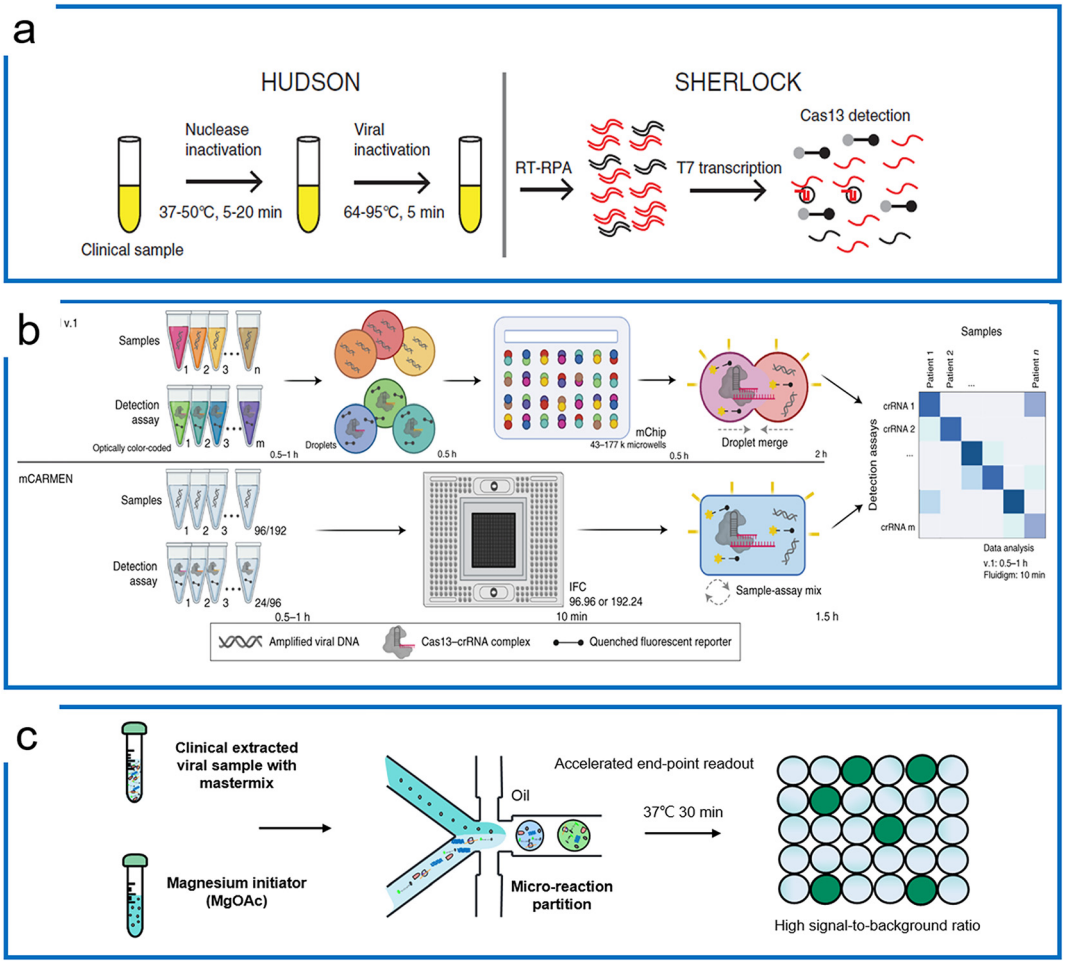

Fig. 5 RPA-based Cas13 diagnostics. (a) The HUDSON protocol that pairs with SHERLOCK for viral detection directly from body fluids; the figure was reproduced from ref. 100 with permission from the American Association for the Advancement of Science, copyright 2018. (b) The massively multiplexed viral detection using Cas13a with microfluidics. The combinatorial droplet merge technique enables amplified targets with droplet color barcodes to merge for multiplexed visualization. The figure was reproduced from ref. 112 under Creative Commons Attribution License from Springer Nature, copyright 2022. (c) Droplet digital quantification with one-pot SHERLOCK. Droplet microfluidics allows the RPA reaction to be triggered after droplets are formed, and enables background-free binarization of droplets where the signals are only triggered by the *trans* reporting of Cas13a in the presence of the desired targets. Adapted from ref. 108 with the permission from American Chemical Society, copyright 2022.

the RPA preamplification starts as soon as the magnesium initiator is added even at ambient temperature, causing premature amplification prior to droplet partitioning.[107] In this method, a Y-shaped microfluidic chip was designed to separate the reaction initiator from the target-included master mix.[108] Moreover, a droplet picoinjector was applied to address this RPA premature amplification, allowing complete premature amplification-free quantification.[73]

3.3.2. Other isothermal amplification assays with Cas13. Apart from the conventional SHERLOCK assay with RPA, the combination of LAMP and Cas13 has also been reported for SARS-CoV-2 detection. Hsu *et al.* have designed a LAMP amplification with the insertion of a T7 transcription sequence for LbuCas13a activation.[109] This workflow includes an RNA extraction-free sample lysis protocol using shelf-stable reagents, LAMP amplification, and Cas13a readout. In addition, LbCas13a has been coupled with RCA for microRNA detection. Even though Cas13a can directly target microRNAs around picomolar sensitivity,[110] it remains challenging to detect target objects with concentrations lower than femtomolar. Thus, the ligation-based RCA method has been designed to amplify the circled templates which were ligated by specific microRNAs. Since the Cas13a only recognizes RNA, the T7 sequence was coded into the padlock probe for RNA transcription, and then the RCA amplicons can be transcribed into activator RNA. This method has thus realized sub-femtomolar sensitivity for microRNA detection, which is 1000 times more sensitive compared with direct detection using LbCas13a.[111]

3.4. Cas12 detection systems with isothermal amplification

Unlike Cas13 which is an RNA targeting system, Cas12 is a DNA targeting system with a *trans*-cleavage ability of ssDNA. Upon the specific binding to the target sequence, Cas12 not only cleaves on the target strand but is activated for

trans-cleavage of the surrounding ssDNA. When bound to dsDNA, the turnover rate of Lbcas12a *trans*-cleavage is over 5-times faster than ssDNA targeting. We summarize the representative Cas12 systems according to the combination of different isothermal amplification methods (see Table 5).

3.4.1. RPA-based Cas12 assays. The discovery of indiscriminate *trans*-cleavage has led to the first isothermal detection method termed DNA endonuclease-targeted CRISPR trans reporter (DETECTR) combined with RPA preamplification (Fig. 6a).[44] DETECTR has been further

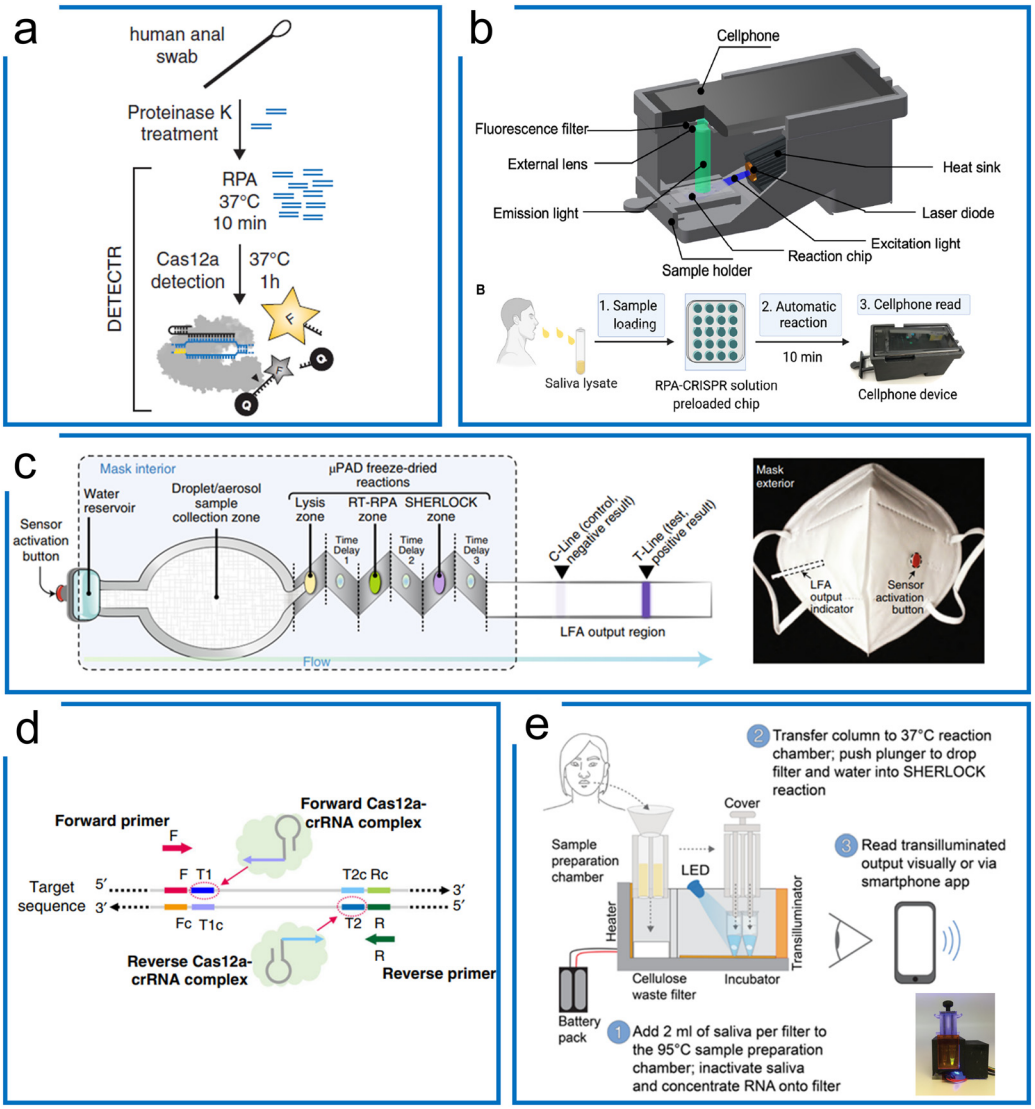

Fig. 6 The RPA-based Cas12a systems for nucleic acid detection. (a) The DETECTR system of Cas12a diagnostics for HPV viral detection, the sample was treated with proteinase K, followed by RPA, and then the targets were detected by Cas12a ribonucleoprotein for *trans*-cleavage of the ssDNA reporters. The figure was reproduced from ref. 44 with permission from the American Association for the Advancement of Science, copyright 2018. (b) A miniaturized system with cell phone readout using the RPA–Cas12a system that allows sensitive and quantitative readout of saliva CRISPR-FDS assays at sites. Sample preparation, amplification, and detection are all combined in one device. The figure was reproduced from ref. 113 under Creative Commons Attribution License from the American Association for the Advancement of Science, copyright 2021. (c) The RPA–Cas12a diagnostics with paper microfluidics in a mask. Once the water reservoir was opened, the target was driven by the capillary force of paper microfluidics through different folded layers for three purposes including sample lysis, RT-RPA amplification, and Cas12a-based detection. All these chemicals associated with these purposes were lyophilized reagents in the mask. The figure was reproduced from ref. 114 with permission from Springer Nature, copyright 2021. (d) A one-pot RPA–Cas12a assay with two targeting sites of crRNAs for enhanced sensitivity of Cas12a diagnosis of COVID-19. After RPA amplification, the amplicons can be targeted using two crRNAs to boost the sensitivity higher compared to the conventional one-crRNA method. The figure was reproduced from ref. 122 under Creative Commons Attribution License from Springer Nature, copyright 2020. (e) A portable device with enhanced one-pot Cas12a and RPA reaction for SARS-CoV-2 and related variants' detection. The target sample was firstly treated with a high temperature for sample preparation, following liquid transfer to another lyophilized power tube to perform the one-pot RPA–Cas12a reaction. Sample preparation, RPA amplification, and Cas12a detection steps were integrated into a small device with a mobile phone readout. The figure was reproduced from ref. 125 under Creative Commons Attribution License from the American Association for the Advancement of Science, copyright 2021.

applied with a smartphone-based miniaturized system to streamline the sample preparation, RPA amplification, and Cas12a detection for the detection of SARS-Cov-2 in saliva without the need for RNA isolation. This platform holds an LOD of 0.38 copies per μL (Fig. 6b).[113] Another Cas12a-based detection method known as the one-hour low-cost multipurpose highly efficient system (HOLMES) that uses PCR as the preamplification has also been reported.[43] Compared to the highly sensitive and specific PCR technology, the combination of RPA and Cas12a increases the isothermal specificity at a single-molecule level without the need for centralized experimental laboratory equipment. Furthermore, the wearable technology was applied with Cas12a to simplify the diagnostic process. Collins *et al.* applied the microfluidic paper-based analytical device (μPAD) with the lyophilized RPA and Cas12a reagents for SARS-COV-2 diagnostics.[114] In this design (Fig. 6c), the sample extraction, RPA preamplification, Cas12a *trans*-cleavage, and LFA visualization were combined into a region of the mask. These assay components in this reaction were driven by the capillary flow with the assistance of a water reservoir on the surface.

Although the RPA and Cas12a combination can achieve high sensitivity and specificity, the multistep process may cause higher cross-contamination risks, alongside the requirement for extra expertise and equipment. Therefore, a one-pot assay of RPA and LbCas12a was developed to fuse the RPA preamplification and CRISPR visualization into a single step. To increase the reported sensitivity, Liu *et al.* designed an approach using two crRNAs for detecting both strands of RPA amplicons (Fig. 6d). They demonstrated that the two-crRNA combination can achieve a higher sensitivity compared to the one-crRNA method. This method achieved 0.33 aM in a one-pot RPA and aCas12a reaction to detect the SARS-Cov-2 N gene within 20 minutes.[122] Besides, Yin *et al.* found that the suboptimal PAM of Cas12a accelerated the reaction with high specificity and sensitivity. Thus, the one-pot RPA and Cas12a reaction uses the suboptimal PAM of Cas12a (*e.g.*, NTTV and TTNT) rather than the canonical PAM (TTTV). This method achieved an LOD of 1 cp μL^{-1} in SARS-COV-2 diagnostics.[123] Comparably, Collins *et al.* optimized reaction factors such as the reaction temperature, reporter concentration, and for RT commercial brands, crRNA and RPA reaction primers, resulting in the improvement of the LOD to 50 aM for *Plasmodium* species in the case of symptomatic and asymptomatic malaria.[124] In another work (Fig. 6e), they further optimized the reaction buffer and enzymes, as well as adding RNase H to improve the RT efficiency for SARS-Cov-2 and related variants. In order to deliver a deployable system, they further developed a minimally instrumented SHERLOCK (miSHERLOCK) POC diagnostic platform, which integrates instrument-free, built-in RNA paper-capture from saliva, room temperature stable reagents, battery-powered incubation, and mobile phone-enabled readout with an LOD of 1000 copies per milliliter.[125]

The one-pot assay has also been extended to digital quantification. Wang *et al.* have applied the nano-well chip for absolute quantification of COVID-19 (ref. 126) and have demonstrated fewer false-positive results. They were able to show that digital detection can be accomplished within 30 minutes to a single-molecule level sensitivity. Yu *et al.* were able to apply yet another commercial digital PCR system for Cas12a and RPA one-pot quantification.[127] This system partitioned the one-pot master mix inside a tube for thousands of partitions similar to nano-well technology. They compared the performance of digital PCR, qPCR, and digital Cas12a and RPA results to demonstrate that this novel technology can be applied to the digital quantification of viral target objects. However, these two technologies have a serious drawback in that the RPA reaction can start at ambient temperature as soon as the magnesium initiator is added,[107,128] which can lead to inaccurate results because of premature amplification during partition.

3.4.2. LAMP-based Cas12 assays. Compared to RPA, which requires multiple enzymes to initiate the amplification process, the LAMP approach only requires one enzyme. The LbCas12a has been coupled with LAMP for SARS-Cov-2 diagnostics in a two-step format. In this protocol, the extracted RNA was firstly amplified by RT-LAMP (Fig. 7a).[129] The Cas12a detection enabled an LFA readout in a commercial strip *via trans*-cleavage, which is accessible and easy-to-use reporting formats such as lateral flow strips, eliminating the need for complex lab infrastructure. The sensitivity and specificity are comparable to the standard PCR protocol of the US Centers for Disease Control (CDC). Moreover, a microfluidic approach of isotachophoresis (ITP) has been reported to streamline viral extraction, LAMP amplification, and Cas12a detection (Fig. 7b).[130] Despite the comparable sensitivity and specificity of this protocol to PCR, this strategy has not been fully integrated into a single chip since LAMP has to be performed off-chip.

Because different reaction temperatures are required for LAMP (~65 °C) and Cas12a (~37 °C), a combined one-pot assay requires the system to be compatible with a wider range of temperatures. Through the screening of the type V enzymes, AacCas12b from *Alicyclobacillus acidoterrestris*, a thermophilic RNA-guided endonuclease that can work around 55 °C, was reported to be first combined with LAMP for a one-pot reaction.[37] However, the sensitivity of this one-pot LAMP and AaCas12b assay is lower compared to the two-step reaction (10 aM). AapCas12b from *Alicyclobacillus acidiphilus* was used by Zhang's group in a one-pot assay working at 60 °C.[50] The guide RNA of AmCas12b was used to guide AapCas12b because the AapCas12b locus does not contain an identifiable CRISPR array.[45] This protocol, termed STOPCovid2 (SHERLOCK Testing in One Pot), has been applied for COVID-19 detection with a 55 zM sensitivity, which is more sensitive compared to the standard PCR test (Fig. 7c). It is notable that whilst the standard LAMP method can generate a nonspecific signal, the STOPCovid only produced a signal in the presence of the target object, which

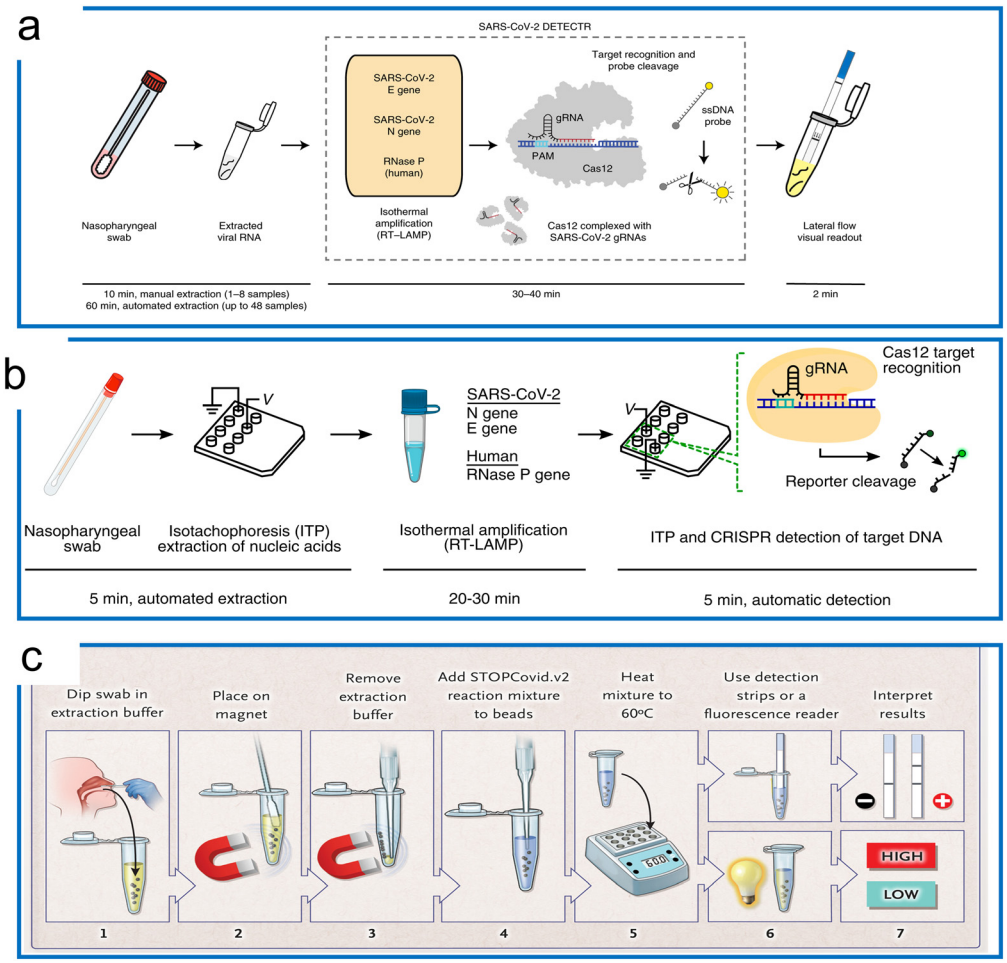

Fig. 7 The LAMP-based Cas12a detection. (a) The DETECTR with the LAMP system for SARS-CoV-2 detection. The traditional RNA extraction method was combined with the LAMP–Cas12a detection scheme. The test results were visualized by either fluorescence or LFA assay. The figure was reproduced from ref. 129 with permission from Springer Nature, copyright 2020. (b) The microfluidic ITP enables COVID-19 detection with LAMP preamplification and Cas12a detection. A streamlined workflow was established with ITP extraction of nucleic acids, off-chip incubation with LAMP, and visualization with Cas12a on an ITP chip. The figure was reproduced from ref. 130 under Creative Commons Attribution License from National Academy of Sciences, copyright 2020. (c) The STOPCovid system with one-pot LAMP and Cas12b for COVID-19 detection. The sample was first collected and treated with extraction buffer assisted by a magnet. Then the lysed target was transferred to perform a LAMP–Cas12b one-pot reaction at 60 °C. Lastly, the readout was conducted using an LFA or fluorescence assay to inspect the results. The figure was reproduced from ref. 50 with permission from Massachusetts Medical Society, copyright 2020.

further indicates that CRISPR detection can enhance the test specificity. Similar work of LAMP using CRISPR–Cas9 to trigger signals only in the presence of the target has also been reported.[131] In addition to the AapCas12b, which has shown excellent performance at a high operation temperature, Nguyen *et al.* recently found that the BrCas12b from *Brevibacillus* sp. exhibited phenomenal stability at high temperatures (*e.g.*, up to 70 °C in the optimal buffers). In combination with LAMP, this thermostable Cas enzyme has been adopted for diagnostics of SARS-COV-2 variants including alpha, beta, gamma, delta, and omicron in a one-pot reaction.[132] The LOD for detection of these variants ranges from 20 aM to 833 aM. Apart from the one-pot reaction that can be utilized for quantification using a standard curve, a LAMP-based LbCas12a reaction has also been developed for digital quantification.[133] The reaction temperature range of LbCas12a can work up to 55 °C. Thus, a dual-priming isothermal amplification (DMAP), a variant of the LAMP method that works at a lower temperature, was designed to combine with LbCas12a for hot-start initiation. The digital quantification using a commercial nano-well chip achieved a 5 cp μL^{-1} sensitivity, which was 10 times higher compared to reactions in bulk.[137]

3.4.3. Other isothermal amplification assays with Cas12a. Cas12a not only enhances reporting *via* collateral activity but also preserves excellent specificity. Hansen *et al.* were able to design a pseudo-circle template that combined the primer generation rolling circle amplification (PG-RCA) with the Cas12a reporting method for a highly sensitive detection down to 1 aM.[134] The nonspecific product made it possible to generate the activator for Cas12a ribonucleoprotein to cleave the specific products. This internal background

control significantly decreased the background noise and kept the test sensitivity due to the unique DNase activity of Cas12a. In the Cas12a ternary system, the main amplification of the target was to generate amplified targets instead of the crRNAs. Liu *et al.* have subsequently been able to apply the rolling circle transcription to generate crRNAs for Cas12a activation using assistant DNA probes.[135] Since the rolling circle transcription (RCT) is a linear amplification method, they further extended this work to hyperbranched rolling circle amplification (HRCA) with the insertion of the T7 sequence for crRNA production, which increased the sensitivity by 47 times.[136] The Cas12a detection system was also integrated with SDA for multistep visualization for ATP and specific gene detection.[137,138]

4 Amplification-free CRISPR detection systems

Although preamplification greatly enhances the sensitivity of the CRISPR diagnostic assays, it inevitably poses limitations to the assay design since additional steps and assay compatibility are required in a more complex system. The amplification-free CRISPR methods present enormous value as testing methods due to their simplicity and rapidity as direct detection platforms. As aforementioned, CRISPR-based diagnostics have a natural sensitivity around the picomolar level using fluorescence measurement.[170] To further increase the sensitivity of amplification-free CRISPR methods, advanced sensing technologies such as surface-enhanced Raman spectroscopy (SERS),[171] electrochemistry,[172] Förster resonance energy transfer (FRET),[173,174] molecular circuits of self-amplification,[175] field-effect transistor (FET),[176,177] tandem crRNA or enzymes,[178,179] *etc.* have been utilized (see a summary of these methods in Table 6). The ability to deploy in resource-limited settings will meet a great need for public health monitoring and general pathogen detection.

4.1. dCas9-based amplification-free assays

The Cas9 system, especially dCas9, is a powerful CRISPR tool for target recognition. The dCas9-based amplification-free schemes apply the programmable recognition ability to identify and enrich the targets before measurement. In general, the dCas9 system can be conjugated with different substrates to immobilize the target oligonucleotide, which can be visualized using different methods including fluorescence,[180] Raman,[181] gFET electrical detection,[176,182] *etc.*

Although the fluorescence *in situ* hybridization (FISH) method enables high-resolution detection of specific DNA in single cells, there are some major drawbacks, such as complex and time-consuming operation, and the need to denature the target DNA. Jung *et al.* have designed a DNA-FISH-based method with dCas9 to detect the dsDNA target within 30 minutes.[180] The hypothesis is that the dCas9–sgRNA complex functions as a targeting material and SYBR Green I (SG I) as a label probe. In this design, the dCas9–sgRNA complex conjugated to a magnetic bead can specifically bind to the target DNA in un-purified cell lysates, and after simple magnet enrichment, SG I staining and washing steps, the LOD of methicillin-resistant *Staphylococcus aureus* (MRSA) detection can reach 10 CFU ml^{-1}.

SERS is a phenomenon where the molecular Raman signal increases near the SERS active surface, which has been applied for nucleic acid detection at single-molecule resolution.[171] Kang *et al.* have been able to introduce SERS into the dCas9 system for the nucleic acid detection of multidrug-resistant bacteria (Fig. 8a). This work combines the specificity of dCas9 and SERS Raman sensitivity. The dCas9–sgRNA complex was first immobilized on gold-coated magnetic nanoparticles (Au MNPs). The dCas9–AuNP complex reacted with the superbugs to recognize the genomic DNA. Then, methylene blue (MB), a Raman reporter, was

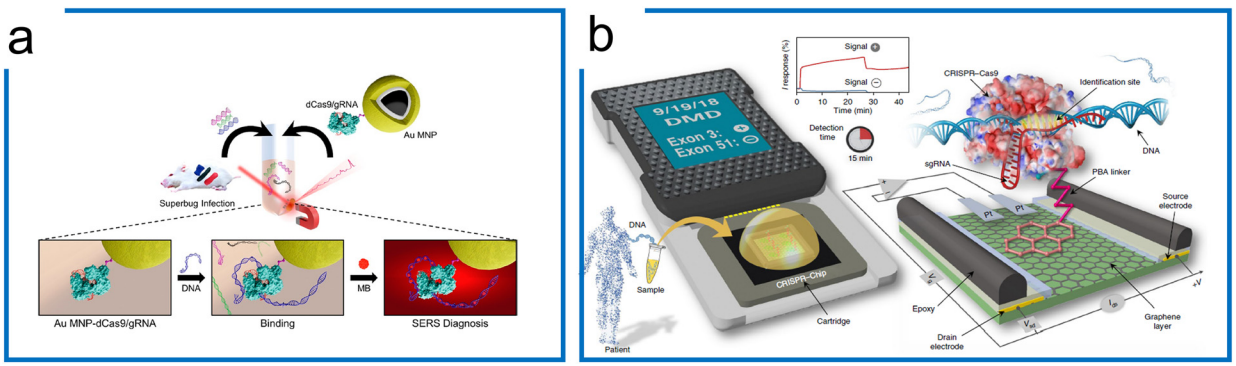

Fig. 8 The amplification-free system with dCas9. (a) A SERS detection strategy with dCas9. The Au MNP-dCas9/gRNA probe can label the genomic DNA of a superbug-infected mouse. MB was introduced to interact with the genomic DNA. After the external magnetic enrichment, the SERS measurement was conducted. Adapted from ref. 181. Copyright 2020 American Chemical Society. (b) A CRISPR-Chip for dsDNA detection. The dCas9 complexed with a target-specific sgRNA (referred to as dRNP) is immobilized on the surface of the graphene within a three-terminal gFET. The dRNP scans the whole genomic DNA and unzips the double helix until it identifies and binds to its target sequence (complementary to the 5′ end of sgRNA). The binding of the target DNA to the dRNP complex can sensitively modulate the electrical characteristics of the gFET, resulting in an electrical signal output within 15 min. The figure was reproduced from ref. 176 with permission from Springer Nature, copyright 2019.

added to this mixture, intercalating into the genomic DNA.[181] By applying an external magnet to collect the dCas9 ternary, the Raman intensity was then measured for target detection. Thus, the SERS coupled with dCas9 is an ultra-sensitive detection method, having an LOD of 8.1fM without amplification.

Apart from the sensitive SERS, a CRISPR-Chip using a graphene-based field-effect transistor (gFET) system was developed (Fig. 8b).[176] Using the gFET as a detection method, CRISPR-Chip can achieve an LOD of 1.7 fM without amplification within 15 min. In this work, the dCas9–sgRNA complex has been linked to the graphene layer with a 1-pyrenebutanoic acid (PBA) linker. The target sequence was bound to the dCas9–sgRNA complex specifically, which enhances the output signal relative to samples lacking the target sequence. To further expand the application of the CRISPR-Chip for SNP detection, two optimizations based on this design were accomplished by (1) monitoring multiple electrical signals including *I*, *C*, and *V* responses, and (2) applying multiple Cas9 orthologs to improve test discrimination.[182]

4.2. Cas12a-based amplification-free assays

Different from tdCas9, which has been widely adopted for sequence labeling and enrichment purposes, the Cas12a system harnesses the *trans*-cleavage ability for amplification-free diagnostics mainly focusing on augmentation of the signal output. Therefore, a series of visualization techniques including electrochemistry,[183–186] LFA,[187] nanoparticle reporter,[188] piezoresistive effect,[189] surface plasmon resonance,[188] and molecular circuits[175,190] have been

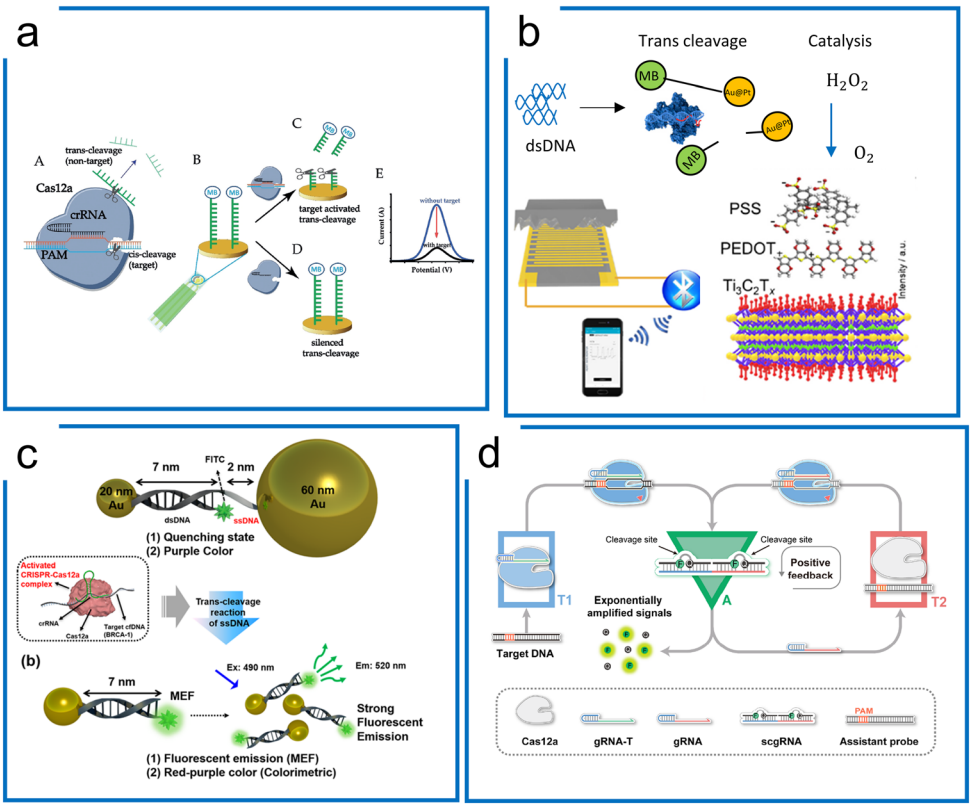

Fig. 9 Amplification-free diagnostics with Cas12. (a) A Cas12a system for dsDNA detection using electrochemistry. MB conjugated ssDNA was immobilized on the electrochemical sensor surface to form the detection machinery. The signal can be measured once Cas12a *trans*-cleaves the ssDNA reporter on the surface of the electrode. The figure was reproduced from ref. 183 with permission from John Wiley and Sons, copyright 2019. (b) The piezoresistive biosensor with Cas12a for HPV-16 detection. When the Cas12a system recognizes the target sequence to activate the *trans*-cleavage, Cas12a enables the separation of AuPt and magnetic beads, which is conjugated *via* ssDNA. The released AuPt catalyzes H_2O_2 into O_2, compressing the piezoresistive sensor to cause the current difference. The figure was reproduced from ref. 189 with permission from Elsevier, copyright 2021. (c) A metal-enhanced fluorescence and colorimetric system with Cas12a. Two different-sized AuNP (20 nm and 60 nm) pairs are connected by DNA hybridization with an ssDNA region to achieve the induction of metal-enhanced fluorescence (MEF) with target DNA and fluorescence quenching in the absence of target DNA. The presence of target DNA enables the *trans*-cleavage of Cas12a *via* the ssDNA region to switch from fluorescence quenching to MEF. Adapted from ref. 188. Copyright 2021 American Chemical Society. (d) A self-amplified system (CONAN) for dsDNA detection, in which a cycling loop is developed after Cas12a recognizes the target sequence. The *trans*-cleavage ability of Cas12a triggers the separation of the RNA–DNA probe to emit fluorescence and a new sgRNA. The released sgRNA guides Cas12a in targeting the assistant probe to release more fluorescence and sgRNA. The figure was reproduced from ref. 175 under Creative Commons Attribution License from the American Association for the Advancement of Science, copyright 2021.

applied to amplify the *trans*-cleavage for enhanced diagnostics.

Liu *et al.* developed an electrochemical biosensor based on CRISPR–Cas12a (E-CRISPR) (Fig. 9a).[183] The ssDNA tagged MBs were first immobilized on the gold electrode as the state condition, whereby the Cas12a ribonucleoprotein binding to the target sequence region then *trans*-cleaves the immobilized ssDNA. The electrical current difference was recorded for diagnostic visualization and an LOD of 50 pM was achieved without amplification.

Tang *et al.* combined the piezoresistive wireless biosensor with Cas12a for HPV diagnosis (Fig. 9b).[189] The *trans*-cleavage ability of Cas12a enables the separation of MB-ssDNA-AuPt reporters upon recognizing the target HPV 16. Subsequently, the separated AuPt particles were enriched by magnetism and then catalyzed H_2O_2 into O_2, which compresses the sensor for increased current, enabling a LOD of 15.22 pM.

Unique surface plasmon resonance properties have also been identified with noble metal nanomaterials (NMNs),[190] which can be regarded as the vibrational motion of an electromagnetic wave propagating in parallel along with the precious metal and dielectric interface. Fluorescence enhancement or fluorescence quenching is exhibited when noble metals are at different distances from the fluorescent dye. Choi *et al.* were able to design a AuNP assisted metal-enhanced fluorescence method for cell-free DNA detection using a Cas12a *trans*-cleavage (in Fig. 9c).[188] A pair of AuNPs of two different sizes (20 nm and 60 nm) is linked through 7 nm long dsDNA and 2 nm long ssDNA, showing fluorescence quenching in the initial state. In the presence of the target DNA, the *trans*-cleavage ability of Cas12a cleaves the non-hybridized ssDNA part to release the 60 nm AuNPs. Therefore, the 20 nm AuNP can induce a strong signal from the fluorophore.

An internal autocatalysis-driven feedback amplification network was designed utilizing Cas12a by Nie *et al.*[175] In this method, the CRISPR–Cas-only amplification network (CONAN) achieves a 5 aM sensitivity without DNA amplification (Fig. 9d). Here, they designed a probe comprising ssDNA reporters binding to the crRNA. When the target was bound to the Cas12a ribonucleoprotein, the probe was cleaved, releasing a fluorescent signal and new crRNA. The released crRNA assembled a new active Cas12a protein and participated in the reaction to achieve autocatalytic signal amplification. Moreover, the entropy driven catalysis DNA networks,[191] as a self-driven amplification method without DNA polymerase, have been integrated with Cas12a for diagnostics and shown to reach picomolar sensitivity.[190]

4.3. Cas13-based amplification-free assays

Cas13 has been widely adopted for direct detection of RNA including mRNAs and microRNAs at picomolar concentrations without amplification. Signal augmentation methods, such as electrochemical biosensors,[194–196] droplet confinement,[193,197,198] and specifically molecular designs, have been combined with Cas13 to increase the LOD.

The confinement of single molecules in cell-like-sized droplets/reactors can enhance local concentrations of the target and reporter by 3 orders of magnitude, and thus may break the detection limit of the most conventional biochemical assays or detectors. Zhou *et al.* achieved >10 000-fold enhancement in sensitivity compared to the bulk Cas13a assay using droplet microfluidics without nucleic acid amplification (Fig. 10a).[192] This work has been further applied to detect SARS-CoV-2 without amplification. Similar work has been demonstrated using a microchamber array to improve the sensitivity of LwCas13a diagnostics down to 5 fM, which is 3 orders of magnitude more sensitive than the bulk test.[198]

Subsequently, Ott *et al.* demonstrated that the combination of multiple crRNAs in the LbuCas13a system can be used to directly detect viral RNA in the attomolar range without amplification. This method integrated with a cell phone readout was used for SARS-CoV-2 detection with a sensitivity of 167 aM within 30 minutes (Fig. 10b).[178] The Cas enzymatic kinetics were found to be associated with the crRNA. Accordingly, Fletcher *et al.* proposed a multiplexed diagnostic method with 2 crRNA that has been used in combination with droplet microfluidics. Based on the stochastic nuclease activities, they analysed the kinetic features of each droplet over time for multiplexing (Fig. 10c).[193]

In addition to the tandem crRNA strategy, the tandem use of unrelated CRISPR nucleases can increase the SHERLOCK sensitivity.[179] Doudna *et al.* engineered the Csm6 with a chemically stabilized activator. Once LbuCas13a guided by multiple crRNAs was activated, the Csm6 would *trans*-cleave extra reporters, creating a one-step amplification-free SARS-CoV-2 detection assay. This method, termed the Fast Integrated Nuclease Detection In Tandem (FIND-IT) approach, enabled an efficient detection (50 aM) within 20 minutes, highlighting the potential for amplification-free RNA detection ability using LbuCas13a (Fig. 10d).

Besides fluorescence visualization, an electrochemical biosensor combined with Cas13a has been reported to directly detect microRNA 19b.[194] In this design, Urban *et al.* were able to immobilize the anti-fluorescein antibodies attached to glucose oxidase (GOx) *via* the FAM and biotin-tagged ssRNA probes on the streptavidin-coated substrate surface. The electrochemical detection was accomplished using GOx to catalyze the substrate, producing H_2O_2, where the current measurement was detected. In the presence of the target microRNA, the activated Cas13a *trans*-cleaved the ssRNA, interrupting the catalytic process. To expand the detection ability, they then further developed a multi-channel microfluidic chip to enable 4 multiple detections.[196] To increase the signal output, a hairpin-based enzyme-free amplification was applied to increase the electrochemical signal *via* a catalytic chain reaction.[199,200]

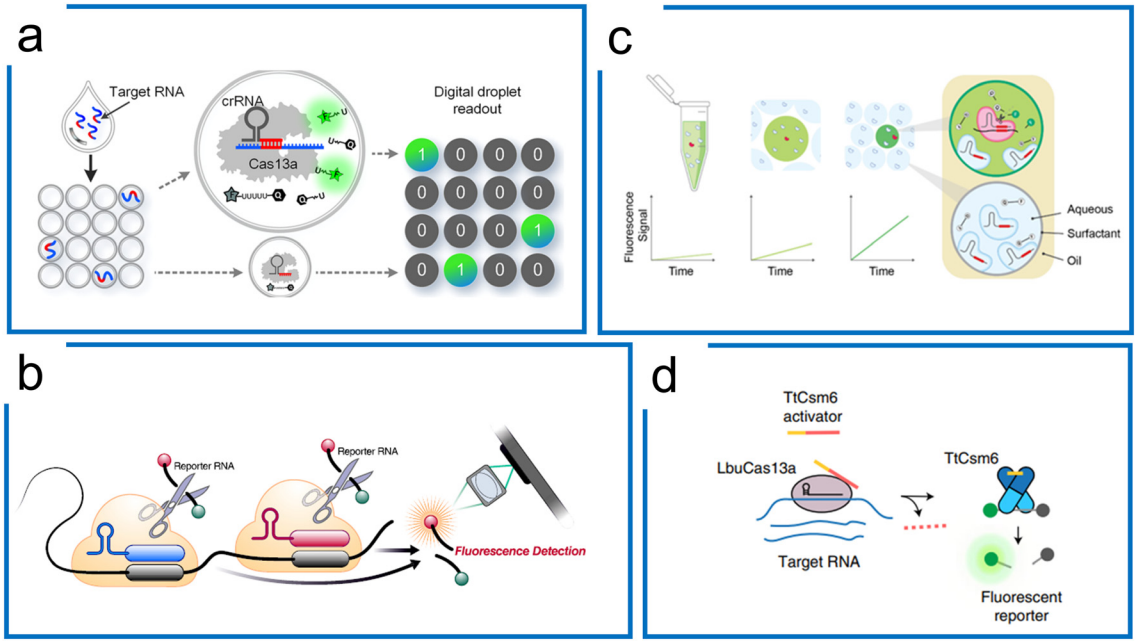

Fig. 10 Cas13a-based amplification-free diagnostics. (a) Droplet microfluidics for Cas13a direct detection of RNA samples. By droplet compartment, local concentrations of the target and reporter are enhanced simultaneously, compared to the bulk Cas13a assay. It enables absolute digital single-molecule RNA quantitation. Adapted from ref. 192. Copyright 2021 American Chemical Society. (b) The tandem crRNAs for SARS-CoV-2 detection. Compared to the single-crRNA guiding Cas13 system, the multiple crRNA for the same target sequence improves the kinetic activity of *trans*-cleavage to higher sensitivity. The figure was reproduced from ref. 178 with permission from Elsevier, copyright 2021. (c) Multiplexed detection using Cas13a kinetic barcodes in droplets. The kinetic difference of Cas13a governed by both target RNA and crRNA is harnessed to achieve multiplexed diagnostics in droplet partition, where the fluorescence trajectory of different micro reactions within the droplets is recorded in real-time to differentiate the different targets. Adapted from ref. 193 under Creative Commons Attribution License from medRxiv. (d) Accelerated RNA detection using tandem CRISPR nucleases. Combining RNA-guided Cas13 and Csm6, a tandem nuclease assay is created with a chemically stabilized activator to achieve both high sensitivity and fast signal generation without requiring a preceding target amplification step. The figure was reproduced from ref. 179 with permission from Springer Nature, copyright 2021.

5 Perspectives

5.1. Target quantification

Accurate quantification of biomarker molecule concentrations is of great importance in order to respond to treatment in companion diagnostic and precision medicine development. Similar to PCR, quantification using a CRISPR-based diagnostics system can be obtained by relative quantification using a standard curve or digital quantification using Poisson statistics.[219] The requirement for quantification through comparison with a standard curve reference and continuous measurement of a signal hampers the feasibility of the CRISPR-based diagnostics system as a POCT tool.

Digital quantification has been reported to greatly reduce uncertainty at low concentrations.[220] By employing nano-well-based[221] or droplet-based[222,223] technologies for sample partitioning, the digital format of CRISPR-based assays enables absolute quantification of nucleic acids with no dependency on endogenous references, as it measures the number of target molecules directly by observing the end-point fluorescence in individual partitions.

To date, most CRISPR effectors in diagnostics operate at ambient temperature. In combination with isothermal amplification, two concerns may arise:[224] target overestimation associated with the premature amplification induced by the near ambient temperature reaction (*e.g.*, RPA-based preamplification) and target loss in the multistep procedures. The possible solutions to address these issues can be classified into three aspects. First, sample preparation at a lower temperature such as in a cold room or on ice and rapid transfer or operation during experiments are demanded. Second, digital quantification reforms from an ambient reaction to a hot-start reaction such as LAMP. With the expansion of the CRISPR Cas family, the thermostability of Cas proteins is discovered.[36,121] Those thermostable proteins of Cas12 and Cas13 families allow the CRISPR diagnostics along with LAMP.[161,225] Finally, the preamplification issue can be avoided by the creation of a reaction initiator (*e.g.*, Mg initiator or DNA polymerase). For instance, the mixing of the MgOAc initiator into the RPA-CRISPR reaction before partitioning can solve the premature amplification using microfluidic technologies such as Y-shaped droplet generator,[108] picoinjector,[226] droplet emerging,[105] droplet array,[104] Slipchip,[227] *etc.* Nevertheless, all the quantification methods require sophisticated ancillary equipment from droplet partition to visualization. The miniaturized and operation-free digital quantification might be another chapter in diagnostics, such as high-throughput

droplet partition,[228–230] vortex droplet partition,[231] advanced pore materials,[232] and self-digitalization systems.[107,233,234]

5.2. Multiplexed detection

Simultaneous diagnosis of multiple targets in one reaction is desirable in order to reduce the overall testing cost and improve the throughput in certain testing demands. With more and more unique properties of Cas enzymes uncovered in recent years, those special features of CRISPR have been leveraged to expand the multiplexing ability of CRISPR diagnostics such as (1) programmable crRNA-based Cas9 system (LEOPARD);[39] (2) orthogonal cleavage properties of Cas enzymes (SHERLOCKv2);[46] (3) droplet barcoding and pairing enabled massively multiplexed detection (CARMEN);[104] (4) heterogeneous nuclease kinetics in a confined volume (droplet kinetic barcoding).[193]

The LEOPARD platform is based on the discovery of the RNA guidance of CjeCas9 derived from cellular RNAs unrelated to viral defense. Thus, the RNA guidance can be reprogrammed to any RNA to affect the activation of CjeCas9 nuclease. This discovery extended the programmability of the spacer region of crRNA to tracrRNA. The sensing of RNA is enabled by creating fluorescent DNA sensors that would be cleaved at a specific locus by Cas9. The current proof-of-principle demonstration of LEOPARD allows the detection of multiple different RNA sequences using gel-based readouts. Alternative methods such as lateral flow and colorimetric readouts would be beneficial for point-of-care detection.

In the Cas12 and Cas13-based detection systems, the signals are normally derived from nonspecific *trans*-cleavage with universal probes, making the multiplexing of various targets a challenging task. In SHERLOCKv2, the Cas13 family has been discovered with the di-nucleotide preference to cleave different sequences. Four Cas13 effectors were discovered to have specific cleavage preferences on di-nucleotide reporters (AU, UC, AC, and GA), and thus their orthogonal collateral-cleavage activities (including Cas13 and Cas12a enzymes) have been harnessed to achieve up to 5 channel multiplexing using distinct fluorescent dyes.[46] Additional multiplexing in a single reaction is possible as newer Cas effectors that possess the di-nucleotide preference are still being explored. However, the combination of multiple nuclease-crRNAs with different probes would be a crowding reaction that may result in high background and low sensitivity.

CARMEN–Cas13 combines the specific sensing ability of the CRISPR-based detection technology SHERLOCK with the throughput capabilities of the combinatorial droplet array technology to enable parallel, scalable, and massively multiplexed diagnostics.[104] To enable high multiplexing with high sample throughput, a set of 1050 color codes was generated using ratios of 4 different fluorescent dyes. Each amplified sample or Cas13 detection mix was emulsified into color-coded droplets. The droplets of all samples and detection mixes were pooled and loaded into a droplet pairing array for registration of the droplet identity with a distinct color code. After the droplet pairs were merged, the Cas13a-triggered fluorescence reported a positive reaction. The high sensitivity and specificity of Cas13a allowed the simultaneous detection of 169 human-associated viruses in a single microchip. An upgraded version of CARMEN (mCARMEN) by leveraging the Fluidigm microfluidic platform has decreased the processing time.[106] Unfortunately, a two-step process is required which compromises its quantification abilities. Future development of one-pot assays or CRISPR-based amplification-free techniques may further simplify mCARMEN. CARMEN or mCARMEN methods have the advantage of extremely high-throughput and multiplex detection capabilities. Further improvements can be focused on the integration and optimization of the multiplexed platforms with advanced microfluidic systems. Similarly, ideas of distributing crRNAs into different microchannels or wells have been developed for the detection of multiple targets using microchip-based space coding.[167]

Droplet microfluidics offers the ability to isolate single molecules and reduce inhibition or interference by confinement as well as accelerated reaction and improved sensitivity in a low reaction volume. Rapid and diverse kinetic activities of the Cas13 reaction were observed when the reaction volume shrank to even a single target in a confined droplet.[196] Thus, this feature is leveraged for multiplexed diagnostics at single-molecule resolution using droplet microfluidics. The kinetic behavior depends on a specific combination of crRNA and its target; thus it can be harnessed for CRISPR-based multiplexed diagnostics by tracking the real-time fluorescence trajectory of individual droplets with single-molecule level sensitivity. As a result, this droplet-based CRISPR/Cas13a assay can realize absolute quantification and multiplexed detection simultaneously. However, this method has only been demonstrated in two-channel multiplexed detection. The multiplexibility might be restricted by the differentiation of the kinetics difference.

5.3. Streamlined point-of-care diagnostics

To date, the majority of efforts in the development of CRISPR-based diagnostic systems have been focused on amplification and detection techniques. For a POCT system, streamlined steps from sample preparation, amplification or amplification-free methods, and signal visualization are all equally important. The nucleic acid preparation can be divided into three steps including target lysis, purification, and elusion. Target lysis then relies on mechanical, chemical, and physical approaches to break the cell membrane and wall to expose the cytoplasm.[235] Some methods have subsequently claimed purification-free nucleic acid detection after lysis.[236–238] However, purification is highly sought after, followed by the elusion step in order to reduce the inhabitation and increase the sensitivity.[239] More recently, the promising thermal lysis method HUDSON has been

developed, which combines the sample preparation and CRISPR isothermal diagnostics for Zika virus and DENV detection at 1 copy per microliter level.[100] Similarly, a chemical-based direct sampling method coupled with LAMP and Cas13 diagnostics has been reported to achieve 25 cp μL^{-1} around 30 min.[240] These methods do not require cumbersome experimental operations such as centrifugal separation used in standard purification protocols, and thus reduce the need for expensive labor force and centralized facilities. These merits imply that the potential POCT with CRISPR could be massively simplified and miniaturized, overcoming the limitations of the PCR system including thermal cycling requirements and inhibitors to DNA polymerase.

Hence, the possible streamlined diagnostics would be *via* either a multistep test kit with easy operations,[241] or an automatic all-in-one system.[109,125] Inspired by the rapid test kit for COVID-19 used massively worldwide, the new detection style is accepted by several with simple liquid handing from the collection of the non-invasive sample into reactions with lyophilized or liquid chemicals. Besides, the ultra-miniaturized system with a simple heating function for sample lysis and incubation and fluorescence reader or LFA visualization are new pathways to further reduce the cost of a POCT device with a more sensitive readout. In addition, a facile and robust molecular assay is highly desired. However, the current one-pot assays have shown less sensitivity compared to the two-step reactions. To address this problem, dedicated optimization of the current molecular reaction schemes and characterization of new Cas effectors are in urgent need for the advancement of POCT.

5.4. Beyond nucleic acid detection

Other than nucleic acids, various biomarkers such as proteins/peptides, small molecules, exosomes, *etc.* are also important sensing targets in environmental protection, microbiome monitoring, food safety, drug testing, and antimicrobial resistance diagnosis. Although CRISPR-based detection schemes cannot be directly applied to non-nucleic acids, the modularity of the CRISPR–Cas system offers a great many opportunities for the development of CRISPR-mediated strategies for sensing non-nucleic-acid targets. The general principle is to convert the non-nucleic-acid targets into pre-designed DNA or RNA intermediates for use of CRISPR–Cas as target-induced ssDNases or RNases. CRISPR–Cas systems coupled with transduction elements including oligonucleotide–protein conjugates,[242–245] aptamers,[246–251] DNAzymes,[252–254] allosteric transcriptional factors,[255,256] riboswitches,[257] and enzymatic reactions[258,259] have been developed for detecting non-nucleic-acid targets. Such developments have expanded the applications of the CRISPR–Cas toolbox to meet diverse purposes such as control of gene expression, nanopore sequencing, live cell imaging, environmental monitoring, *etc.*

However, due to the lack of inherent mechanisms for the amplification of non-nucleic-acid targets, the detection limit of non-nucleic-acid targets by CRISPR systems is still comparably inferior, pending more innovative coupling and integration techniques with advanced sensing instruments. Moreover, simultaneous detection of multiple non-nucleic-acid targets remains a challenge and the development of such schemes is still in its infancy. Various approaches, such as assorted labeling and barcoding strategies, super-resolution imaging, microfluidics, microarrays, *etc.*, should be explored for multi-target sensing or fit-for-purpose applications.

6 Conclusions

In this review, we discuss the developments of CRISPR-based detection strategies utilizing different Cas subsystems, the mechanisms of CRISPR/Cas as elegant molecular scissors that recognize and cut nucleic acid targets, and the engineering of such molecular scissors for a broader detection of biomolecules with flexibility, sensitivity, and specificity. The coupling of CRISPR–Cas enzymes with either nuclei acid amplification or signal amplification methods has provided us flexible choices of schemes to meet the detection requirements in terms of the types of targets and sensitivity needed. Besides, the development of direct targeting using CRISPR with new signal transformation schemes has shown a blooming prosperity of this field to avoid enzyme-based amplification methods. Moreover, the advancement of emerging technologies such as nanotechnologies, microfluidics, and wearable electronics will continuously propel the CRISPR-based technologies towards rapid, high-throughput, integrated, multiplexed, and digital detection. However, the practical applications have to wait for a little bit longer till the chemical stability (*e.g.*, crRNAs, enzymes), storage, and overall design of easy-to-use schemes can be fully achieved. Combining microfluidics, wearable technology, flexible materials, and nanotechnology, CRISPR-based technologies will lead to many powerful POCT devices meeting the growing necessity for quick, accurate and resource-limited medical tests to help quickly respond to outbreaks of viral and other diseases.

Conflicts of interest

There are no conflicts to declare.

Acknowledgements

This work was supported by the Research Grants Council of Hong Kong under the General Research Fund (16205619) and the Collaborative Research Fund (C6107-20GF), and the Innovation and Technology Commission under Midstream Research Programme for Universities (MRP/077/20).

Notes and references

1 C. Wang, P. W. Horby, F. G. Hayden and G. F. Gao, *Lancet*, 2020, **395**, 470–473.
2 D. S. Chertow, *Science*, 2018, **360**, 381–382.
3 R. Barrangou, C. Fremaux, H. Deveau, M. Richards, P. Boyaval, S. Moineau, D. A. Romero and P. Horvath, *Science*, 2007, **315**, 1709–1712.
4 K. S. Makarova, Y. I. Wolf, O. S. Alkhnbashi, F. Costa, S. A. Shah, S. J. Saunders, R. Barrangou, S. J. Brouns, E. Charpentier and D. H. Haft, *Nat. Rev. Microbiol.*, 2015, **13**, 722–736.
5 P. Mohanraju, K. S. Makarova, B. Zetsche, F. Zhang, E. V. Koonin and J. Van der Oost, *Science*, 2016, **353**(6299), aad5147.
6 S. A. Jackson, R. E. McKenzie, R. D. Fagerlund, S. N. Kieper, P. C. Fineran and S. J. Brouns, *Science*, 2017, **356**, eaal5056.
7 R. Barrangou and P. Horvath, *Nat. Microbiol.*, 2017, **2**, 1–9.
8 J. McGinn and L. A. Marraffini, *Nat. Rev. Microbiol.*, 2019, **17**, 7–12.
9 K. S. Makarova, Y. I. Wolf, J. Iranzo, S. A. Shmakov, O. S. Alkhnbashi, S. J. Brouns, E. Charpentier, D. Cheng, D. H. Haft and P. Horvath, *Nat. Rev. Microbiol.*, 2020, **18**, 67–83.
10 Y. Ishino, H. Shinagawa, K. Makino, M. Amemura and A. Nakata, *J. Bacteriol.*, 1987, **169**, 5429–5433.
11 M. Jinek, K. Chylinski, I. Fonfara, M. Hauer, J. A. Doudna and E. Charpentier, *Science*, 2012, **337**, 816–821.
12 K. Pardee, A. A. Green, M. K. Takahashi, D. Braff, G. Lambert, J. W. Lee, T. Ferrante, D. Ma, N. Donghia, M. Fan and J. J. Collins, *Cell*, 2016, **165**, 1255–1266.
13 L. Cong, F. A. Ran, D. Cox, S. Lin, R. Barretto, N. Habib, P. D. Hsu, X. Wu, W. Jiang and L. A. Marraffini, *Science*, 2013, **339**, 819–823.
14 J. Quan, C. Langelier, A. Kuchta, J. Batson, N. Teyssier, A. Lyden, S. Caldera, A. McGeever, B. Dimitrov and R. King, *Nucleic Acids Res.*, 2019, **47**, e83.
15 P. Giesselmann, B. Brändl, E. Raimondeau, R. Bowen, C. Rohrandt, R. Tandon, H. Kretzmer, G. Assum, C. Galonska and R. Siebert, *Nat. Biotechnol.*, 2019, **37**, 1478–1481.
16 T. Gilpatrick, I. Lee, J. E. Graham, E. Raimondeau, R. Bowen, A. Heron, B. Downs, S. Sukumar, F. J. Sedlazeck and W. Timp, *Nat. Biotechnol.*, 2020, **38**, 433–438.
17 O. O. Abudayyeh, J. S. Gootenberg, S. Konermann, J. Joung, I. M. Slaymaker, D. B. Cox, S. Shmakov, K. S. Makarova, E. Semenova and L. Minakhin, *Science*, 2016, **353**(6299), aaf5573.
18 A. East-Seletsky, M. R. O'Connell, S. C. Knight, D. Burstein, J. H. Cate, R. Tjian and J. A. Doudna, *Nature*, 2016, **538**, 270–273.
19 B. Perez-Lopez and M. Mir, *Talanta*, 2021, **225**, 121898.
20 Y. Tang, L. Gao, W. Feng, C. Guo, Q. Yang, F. Li and X. C. Le, *Chem. Soc. Rev.*, 2021, **50**, 11844.
21 H. Rahimi, M. Salehiabar, M. Barsbay, M. Ghaffarlou, T. Kavetskyy, A. Sharafi, S. Davaran, S. C. Chauhan, H. Danafar and S. Kaboli, *ACS Sens.*, 2021, **6**, 1430–1445.
22 M. M. Kaminski, O. O. Abudayyeh, J. S. Gootenberg, F. Zhang and J. J. Collins, *Nat. Biomed. Eng.*, 2021, **5**, 643–656.
23 P. Li, H. Xiong, B. Yang, X. Jiang, J. Kong and X. Fang, *TrAC, Trends Anal. Chem.*, 2022, 116812.
24 Y. Dai, Y. Wu, G. Liu and J. J. Gooding, *Angew. Chem., Int. Ed.*, 2020, **59**, 20754–20766.
25 Y. Chen, S. Qian, X. Yu, J. Wu and J. Xu, *Trends Biotechnol.*, 2022, DOI: **10.1016/j.tibtech.2022.07.015**.
26 J. E. van Dongen, J. T. Berendsen, R. D. Steenbergen, R. M. Wolthuis, J. C. Eijkel and L. I. Segerink, *Biosens. Bioelectron.*, 2020, **166**, 112445.
27 H. Yue, M. Huang, T. Tian, E. Xiong and X. Zhou, *ACS Nano*, 2021, **15**, 7848–7859.
28 R. Nouri, Z. Tang, M. Dong, T. Liu, A. Kshirsagar and W. Guan, *Biosens. Bioelectron.*, 2021, **178**, 113012.
29 A. Lau, C. Ren and L. P. Lee, *Shengwu Yixue Gongchengxue Jinzhan*, 2020, **3**, 012001.
30 J. A. Steens, Y. Zhu, D. W. Taylor, J. P. Bravo, S. H. Prinsen, C. D. Schoen, B. J. Keijser, M. Ossendrijver, L. M. Hofstra and S. J. Brouns, *Nat. Commun.*, 2021, **12**, 1–12.
31 K. Yoshimi, K. Takeshita, S. Yamayoshi, S. Shibumura, Y. Yamauchi, M. Yamamoto, H. Yotsuyanagi, Y. Kawaoka and T. Mashimo, *iScience*, 2022, **25**, 103830.
32 D. A. Huyke, A. Ramachandran, V. I. Bashkirov, E. K. Kotseroglou, T. Kotseroglou and J. G. Santiago, *Anal. Chem.*, 2022, **94**, 9826–9834.
33 A. S. Avaro and J. G. Santiago, *Angew. Chem., Int. Ed.*, 2022, **61**, e202209527.
34 A. Ramachandran and J. G. Santiago, *Anal. Chem.*, 2021, **93**, 7456–7464.
35 F. Teng, T. Cui, G. Feng, L. Guo, K. Xu, Q. Gao, T. Li, J. Li, Q. Zhou and W. Li, *Cell Discovery*, 2018, **4**, 1–15.
36 L. T. Nguyen, N. C. Macaluso, B. L. Pizzano, M. N. Cash, J. Spacek, J. Karasek, M. R. Miller, J. A. Lednicky, R. R. Dinglasan and M. Salemi, *EBioMedicine*, 2022, **77**, 103926.
37 L. Li, S. Li, N. Wu, J. Wu, G. Wang, G. Zhao and J. Wang, *ACS Synth. Biol.*, 2019, **8**, 2228–2237.
38 M. R. O'Connell, B. L. Oakes, S. H. Sternberg, A. East-Seletsky, M. Kaplan and J. A. Doudna, *Nature*, 2014, **516**, 263–266.
39 C. Jiao, S. Sharma, G. Dugar, N. L. Peeck, T. Bischler, F. Wimmer, Y. Yu, L. Barquist, C. Schoen and O. Kurzai, *Science*, 2021, **372**, 941–948.
40 L. S. Qi, M. H. Larson, L. A. Gilbert, J. A. Doudna, J. S. Weissman, A. P. Arkin and W. A. Lim, *Cell*, 2013, **152**, 1173–1183.
41 J. S. Gootenberg, O. O. Abudayyeh, J. W. Lee, P. Essletzbichler, A. J. Dy, J. Joung, V. Verdine, N. Donghia, N. M. Daringer and C. A. Freije, *Science*, 2017, **356**, 438–442.
42 M. J. Kellner, J. G. Koob, J. S. Gootenberg, O. O. Abudayyeh and F. Zhang, *Nat. Protoc.*, 2019, **14**, 2986–3012.
43 S. Li, Q. Cheng, J. Wang, X. Li, Z. Zhang, S. Gao, R. Cao, G. Zhao and J. Wang, *Cell Discovery*, 2018, **4**, 1–4.
44 J. S. Chen, E. Ma, L. B. Harrington, M. Da Costa, X. Tian, J. M. Palefsky and J. A. Doudna, *Science*, 2018, **360**, 436–439.
45 P. Ma, Q. Meng, B. Sun, B. Zhao, L. Dang, M. Zhong, S. Liu, H. Xu, H. Mei and J. Liu, *Adv. Sci.*, 2020, **7**, 2001300.

46 J. S. Gootenberg, O. O. Abudayyeh, M. J. Kellner, J. Joung, J. J. Collins and F. Zhang, *Science*, 2018, **360**, 439–444.
47 L. T. Nguyen, B. M. Smith and P. K. Jain, *Nat. Commun.*, 2020, **11**, 1–13.
48 H. Yang, P. Gao, K. R. Rajashankar and D. J. Patel, *Cell*, 2016, **167**, 1814–1828, e12.
49 J. Strecker, S. Jones, B. Koopal, J. Schmid-Burgk, B. Zetsche, L. Gao, K. S. Makarova, E. V. Koonin and F. Zhang, *Nat. Commun.*, 2019, **10**, 1–8.
50 J. Joung, A. Ladha, M. Saito, N. Kim, A. E. Woolley, M. Segel, R. P. Barretto, A. Ranu, R. K. Macrae, G. Faure and F. Zhang, *N. Engl. J. Med.*, 2020, **383**, 1492–1494.
51 F. Teng, L. Guo, T. Cui, X. Wang, K. Xu, Q. Gao, Q. Zhou and W. Li, *Genome Biol.*, 2019, **20**, 1–7.
52 L. B. Harrington, D. Burstein, J. S. Chen, D. Paez-Espino, E. Ma, I. P. Witte, J. C. Cofsky, N. C. Kyrpides, J. F. Banfield and J. A. Doudna, *Science*, 2018, **362**, 839–842.
53 T. Karvelis, G. Bigelyte, J. K. Young, Z. Hou, R. Zedaveinyte, K. Budre, S. Paulraj, V. Djukanovic, S. Gasior and A. Silanskas, *Nucleic Acids Res.*, 2020, **48**, 5016–5023.
54 O. O. Abudayyeh, J. S. Gootenberg, P. Essletzbichler, S. Han, J. Joung, J. J. Belanto, V. Verdine, D. B. Cox, M. J. Kellner and A. Regev, *Nature*, 2017, **550**, 280–284.
55 A. East-Seletsky, M. R. O'Connell, D. Burstein, G. J. Knott and J. A. Doudna, *Mol. Cell*, 2017, **66**, 373–383, e3.
56 T. Notomi, H. Okayama, H. Masubuchi, T. Yonekawa, K. Watanabe, N. Amino and T. Hase, *Nucleic Acids Res.*, 2000, **28**, e63.
57 O. Piepenburg, C. H. Williams, D. L. Stemple and N. A. Armes, *PLoS Biol.*, 2006, **4**, e204.
58 G. T. Walker, M. S. Fraiser, J. L. Schram, M. C. Little, J. G. Nadeau and D. P. Malinowski, *Nucleic Acids Res.*, 1992, **20**, 1691–1696.
59 J. Compton, *Nature*, 1991, **350**, 91–92.
60 J. Van Ness, L. K. Van Ness and D. J. Galas, *Proc. Natl. Acad. Sci. U. S. A.*, 2003, **100**, 4504–4509.
61 P. M. Lizardi, X. Huang, Z. Zhu, P. Bray-Ward, D. C. Thomas and D. C. Ward, *Nat. Genet.*, 1998, **19**, 225–232.
62 A. Ganguli, A. Mostafa, J. Berger, M. Y. Aydin, F. Sun, S. A. Stewart de Ramirez, E. Valera, B. T. Cunningham, W. P. King and R. Bashir, *Proc. Natl. Acad. Sci. U. S. A.*, 2020, **117**, 22727–22735.
63 V. L. D. Thi, K. Herbst, K. Boerner, M. Meurer, L. P. Kremer, D. Kirrmaier, A. Freistaedter, D. Papagiannidis, C. Galmozzi and M. L. Stanifer, *Sci. Transl. Med.*, 2020, **12**, eabc7075.
64 B. A. Rabe and C. Cepko, *Proc. Natl. Acad. Sci. U. S. A.*, 2020, **117**, 24450–24458.
65 M. El-Tholoth, H. H. Bau and J. Song, *ChemRxiv*, 2020, preprint, DOI: **10.26434/chemrxiv.11860137.v1**.
66 T. Chaibun, J. Puenpa, T. Ngamdee, N. Boonapatcharoen, P. Athamanolap, A. P. O'Mullane, S. Vongpunsawad, Y. Poovorawan, S. Y. Lee and B. Lertanantawong, *Nat. Commun.*, 2021, **12**, 1–10.
67 B. Tian, F. Gao, J. Fock, M. Dufva and M. F. Hansen, *Biosens. Bioelectron.*, 2020, **165**, 112356.
68 Q. Wu, C. Suo, T. Brown, T. Wang, S. A. Teichmann and A. R. Bassett, *Sci. Adv.*, 2021, **7**, eabe5054.
69 J. G. Carter, L. O. Iturbe, J. H. Duprey, I. R. Carter, C. D. Southern, M. Rana, C. M. Whalley, A. Bosworth, A. D. Beggs, M. R. Hicks, J. H. Tucker and T. R. Dafforn, *Proc. Natl. Acad. Sci. U. S. A.*, 2021, **118**(35), e2100347118.
70 Y. Zhao, F. Chen, Q. Li, L. Wang and C. Fan, *Chem. Rev.*, 2015, **115**, 12491–12545.
71 M. L. Powell, F. R. Bowler, A. J. Martinez, C. J. Greenwood, N. Armes and O. Piepenburg, *Anal. Biochem.*, 2018, **543**, 108–115.
72 X. Lu, H. L. Yu, H. Lin, Y. Cao and I. Hsing, *Sens. Actuators, B*, 2022, 131385.
73 J. Q. Cui, F. X. Liu, H. Park, K. W. Chan, T. Leung, B. Z. Tang and S. Yao, *Biosens. Bioelectron.*, 2022, 114019.
74 J. C. Guatelli, K. M. Whitfield, D. Y. Kwoh, K. J. Barringer, D. D. Richman and T. R. Gingeras, *Proc. Natl. Acad. Sci. U. S. A.*, 1990, **87**, 1874–1878.
75 G. T. Walker, M. C. Little, J. G. Nadeau and D. D. Shank, *Proc. Natl. Acad. Sci. U. S. A.*, 1992, **89**, 392–396.
76 F. B. Dean, J. R. Nelson, T. L. Giesler and R. S. Lasken, *Genome Res.*, 2001, **11**, 1095–1099.
77 N. Tomita, Y. Mori, H. Kanda and T. Notomi, *Nat. Protoc.*, 2008, **3**, 877–882.
78 H. Jia, Z. Li, C. Liu and Y. Cheng, *Angew. Chem., Int. Ed.*, 2010, **49**, 5498–5501.
79 W. Zhou, L. Hu, L. Ying, Z. Zhao, P. K. Chu and X. Yu, *Nat. Commun.*, 2018, **9**, 1–11.
80 M. Huang, X. Zhou, H. Wang and D. Xing, *Anal. Chem.*, 2018, **90**, 2193–2200.
81 M. S. Reid, X. C. Le and H. Zhang, *Angew. Chem., Int. Ed.*, 2018, **57**, 11856–11866.
82 T. Wang, Y. Liu, H. Sun, B. Yin and B. Ye, *Angew. Chem.*, 2019, **131**, 5436–5440.
83 L. Wang, X. Shen, T. Wang, P. Chen, N. Qi, B. Yin and B. Ye, *Biosens. Bioelectron.*, 2020, **165**, 112364.
84 K. Zhang, R. Deng, X. Teng, Y. Li, Y. Sun, X. Ren and J. Li, *J. Am. Chem. Soc.*, 2018, **140**, 11293–11301.
85 X. Wang, E. Xiong, T. Tian, M. Cheng, W. Lin, H. Wang, G. Zhang, J. Sun and X. Zhou, *ACS Nano*, 2020, **14**, 2497–2508.
86 E. Xiong, L. Jiang, T. Tian, M. Hu, H. Yue, M. Huang, W. Lin, Y. Jiang, D. Zhu and X. Zhou, *Angew. Chem.*, 2021, **133**, 5367–5375.
87 X. Qiu, L. Zhu, C. Zhu, J. Ma, T. Hou, X. Wu, S. Xie, L. Min, D. Tan and D. Zhang, *ACS Synth. Biol.*, 2018, **7**, 807–813.
88 T. Marsic, Z. Ali, M. Tehseen, A. Mahas, S. Hamdan and M. Mahfouz, *Nano Lett.*, 2021, **21**, 3596–3603.
89 Z. Ali, E. Sánchez, M. Tehseen, A. Mahas, T. Marsic, R. Aman, G. Sivakrishna Rao, F. S. Alhamlan, M. S. Alsanea and A. A. Al-Qahtani, *ACS Synth. Biol.*, 2022, **11**, 406–419.
90 B. Koo, D. Kim, J. Kweon, C. E. Jin, S. Kim, Y. Kim and Y. Shin, *Sens. Actuators, B*, 2018, **273**, 316–321.
91 R. Wang, X. Zhao, X. Chen, X. Qiu, G. Qing, H. Zhang, L. Zhang, X. Hu, Z. He and D. Zhong, *Anal. Chem.*, 2019, **92**, 2176–2185.

92 Y. Bao, Y. Jiang, E. Xiong, T. Tian, Z. Zhang, J. Lv, Y. Li and X. Zhou, *ACS Sens.*, 2020, **5**, 1082–1091.
93 X. Sun, Y. Wang, L. Zhang, S. Liu, M. Zhang, J. Wang, B. Ning, Y. Peng, J. He and Y. Hu, *Anal. Chem.*, 2020, **92**, 3032–3041.
94 M. Chen, D. Wu, S. Tu, C. Yang, D. Chen and Y. Xu, *Biosens. Bioelectron.*, 2021, **173**, 112821.
95 M. Azhar, R. Phutela, M. Kumar, A. H. Ansari, R. Rauthan, S. Gulati, N. Sharma, D. Sinha, S. Sharma and S. Singh, *Biosens. Bioelectron.*, 2021, **183**, 113207.
96 T. Marsic, Z. Ali, M. Tehseen, A. Mahas, S. Hamdan and M. Mahfouz, *Nano Lett.*, 2021, **21**, 3596–3603.
97 M. Bengtson, M. Bharadwaj, O. Franch, J. van der Torre, V. Meerdink, H. Schallig and C. Dekker, *Nanoscale*, 2022, **14**, 1885–1895.
98 T. Wang, Y. Wang, P. Chen, B. Yin and B. Ye, *Anal. Chem.*, 2022, **94**, 12461–12471.
99 J. Song, B. Cha, J. Moon, H. Jang, S. Kim, J. Jang, D. Yong, H. Kwon, I. Lee and E. Lim, *ACS Nano*, 2022, **16**, 11300–11314.
100 C. Myhrvold, C. A. Freije, J. S. Gootenberg, O. O. Abudayyeh, H. C. Metsky, A. F. Durbin, M. J. Kellner, A. L. Tan, L. M. Paul and L. A. Parham, *Science*, 2018, **360**, 444–448.
101 K. G. Barnes, A. E. Lachenauer, A. Nitido, S. Siddiqui, R. Gross, B. Beitzel, K. J. Siddle, C. A. Freije, B. Dighero-Kemp and S. B. Mehta, *Nat. Commun.*, 2020, **11**, 1–10.
102 J. Arizti-Sanz, C. A. Freije, A. C. Stanton, B. A. Petros, C. K. Boehm, S. Siddiqui, B. M. Shaw, G. Adams, T. F. Kosoko-Thoroddsen and M. E. Kemball, *Nat. Commun.*, 2020, **11**, 1–9.
103 H. C. Metsky, N. L. Welch, P. P. Pillai, N. J. Haradhvala, L. Rumker, S. Mantena, Y. B. Zhang, D. K. Yang, C. M. Ackerman and J. Weller, *Nat. Biotechnol.*, 2022, 1–9.
104 C. M. Ackerman, C. Myhrvold, S. G. Thakku, C. A. Freije, H. C. Metsky, D. K. Yang, H. Y. Simon, C. K. Boehm, T. F. Kosoko-Thoroddsen and J. Kehe, *Nature*, 2020, **582**, 277–282.
105 A. Kulesa, J. Kehe, J. E. Hurtado, P. Tawde and P. C. Blainey, *Proc. Natl. Acad. Sci. U. S. A.*, 2018, **115**, 6685–6690.
106 N. L. Welch, M. Zhu, C. Hua, J. Weller, M. E. Mirhashemi, T. G. Nguyen, S. Mantena, M. R. Bauer, B. M. Shaw, C. M. Ackerman and C. Myhrvold, *Nat. Med.*, 2022, 1.
107 E. Yeh, C. Fu, L. Hu, R. Thakur, J. Feng and L. P. Lee, *Sci. Adv.*, 2017, **3**, e1501645.
108 F. X. Liu, J. Q. Cui, H. Park, K. W. Chan, T. Leung, B. Z. Tang and S. Yao, *Anal. Chem.*, 2022, **94**, 5883–5892.
109 S. S. Chandrasekaran, S. Agrawal, A. Fanton, A. R. Jangid, B. Charrez, A. M. Escajeda, S. Son, R. Mcintosh, H. Tran, A. Bhuiya and P. D. Hsu, *Nat. Biomed. Eng.*, 2022, 1–13.
110 Y. Shan, X. Zhou, R. Huang and D. Xing, *Anal. Chem.*, 2019, **91**, 5278–5285.
111 M. Huang, R. Huang, H. Yue, Y. Shan and D. Xing, *Sens. Actuators, B*, 2020, **325**, 128799.
112 N. L. Welch, M. Zhu, C. Hua, J. Weller, M. E. Mirhashemi, T. G. Nguyen, S. Mantena, M. R. Bauer, B. M. Shaw and C. M. Ackerman, *Nat. Med.*, 2022, 1–12.
113 B. Ning, T. Yu, S. Zhang, Z. Huang, D. Tian, Z. Lin, A. Niu, N. Golden, K. Hensley and B. Threeton, *Sci. Adv.*, 2021, **7**, eabe3703.
114 P. Q. Nguyen, L. R. Soenksen, N. M. Donghia, N. M. Angenent-Mari, H. de Puig, A. Huang, R. Lee, S. Slomovic, T. Galbersanini, G. Lansberry and J. J. Collins, *Nat. Biotechnol.*, 2021, **39**, 1366–1374.
115 C. Yuan, T. Tian, J. Sun, M. Hu, X. Wang, E. Xiong, M. Cheng, Y. Bao, W. Lin and J. Jiang, *Anal. Chem.*, 2020, **92**, 4029–4037.
116 M. M. Kaminski, M. A. Alcantar, I. T. Lape, R. Greensmith, A. C. Huske, J. A. Valeri, F. M. Marty, V. Klämbt, J. Azzi and E. Akalin, *Nat. Biomed. Eng.*, 2020, **4**, 601–609.
117 M. Patchsung, K. Jantarug, A. Pattama, K. Aphicho, S. Suraritdechachai, P. Meesawat, K. Sappakhaw, N. Leelahakorn, T. Ruenkam and T. Wongsatit, *Nat. Biomed. Eng.*, 2020, **4**, 1140–1149.
118 J. Arizti-Sanz, A. Bradley, Y. B. Zhang, C. K. Boehm, C. A. Freije, M. E. Grunberg, T. F. Kosoko-Thoroddsen, N. L. Welch, P. P. Pillai and S. Mantena, *Nat. Biomed. Eng.*, 2022, 1–12.
119 M. Patchsung, A. Homchan, K. Aphicho, S. Suraritdechachai, T. Wanitchanon, A. Pattama, K. Sappakhaw, P. Meesawat, T. Wongsatit and A. Athipanyasilp, *medRxiv*, 2022, preprint, DOI: **10.1101/2022.03.17.22272589**.
120 B. Casati, J. P. Verdi, A. Hempelmann, M. Kittel, A. G. Klaebisch, B. Meister, S. Welker, S. Asthana, S. Di Giorgio and P. Boskovic, *Nat. Commun.*, 2022, **13**, 1–11.
121 A. Mahas, T. Marsic, M. Lopez-Portillo Masson, Q. Wang, R. Aman, C. Zheng, Z. Ali, M. Alsanea, A. Al-Qahtani and B. Ghanem, *Proc. Natl. Acad. Sci. U. S. A.*, 2022, **119**, e2118260119.
122 X. Ding, K. Yin, Z. Li, R. V. Lalla, E. Ballesteros, M. M. Sfeir and C. Liu, *Nat. Commun.*, 2020, **11**, 1–10.
123 S. Lu, X. Tong, Y. Han, K. Zhang, Y. Zhang, Q. Chen, J. Duan, X. Lei, M. Huang and Y. Qiu, *Nat. Biomed. Eng.*, 2022, 1–12.
124 R. A. Lee, H. De Puig, P. Q. Nguyen, N. M. Angenent-Mari, N. M. Donghia, J. P. McGee, J. D. Dvorin, C. M. Klapperich, N. R. Pollock and J. J. Collins, *Proc. Natl. Acad. Sci. U. S. A.*, 2020, **117**, 25722–25731.
125 H. de Puig, R. A. Lee, D. Najjar, X. Tan, L. R. Soenksen, N. M. Angenent-Mari, N. M. Donghia, N. E. Weckman, A. Ory and C. F. Ng, *Sci. Adv.*, 2021, **7**, eabh2944.
126 J. S. Park, K. Hsieh, L. Chen, A. Kaushik, A. Y. Trick and T. Wang, *Adv. Sci.*, 2021, **8**, 2003564.
127 X. Wu, J. K. Tay, C. K. Goh, C. Chan, Y. H. Lee, S. L. Springs, K. S. Loh, T. K. Lu and H. Yu, *Biomaterials*, 2021, **274**, 120876.
128 J. Li, J. Macdonald and F. von Stetten, *Analyst*, 2018, **144**, 31–67.
129 J. P. Broughton, X. Deng, G. Yu, C. L. Fasching, V. Servellita, J. Singh, X. Miao, J. A. Streithorst, A. Granados and A. Sotomayor-Gonzalez, *Nat. Biotechnol.*, 2020, **38**, 870–874.
130 A. Ramachandran, D. A. Huyke, E. Sharma, M. K. Sahoo, C. Huang, N. Banaei, B. A. Pinsky and J. G. Santiago, *Proc. Natl. Acad. Sci. U. S. A.*, 2020, **117**, 29518–29525.

131 Y. Bao, Y. Jiang, E. Xiong, T. Tian, Z. Zhang, J. Lv, Y. Li and X. Zhou, *ACS Sens.*, 2020, **5**, 1082–1091.
132 L. T. Nguyen, N. C. Macaluso, B. L. Pizzano, M. N. Cash, J. Spacek, J. Karasek, M. R. Miller, J. A. Lednicky, R. R. Dinglasan and M. Salemi, *EBioMedicine*, 2022, **77**, 103926.
133 X. Ding, K. Yin, Z. Li, M. M. Sfeir and C. Liu, *Biosens. Bioelectron.*, 2021, **184**, 113218.
134 B. Tian, G. A. S. Minero, J. Fock, M. Dufva and M. F. Hansen, *Nucleic Acids Res.*, 2020, **48**, e30.
135 G. Wang, W. Tian, X. Liu, W. Ren and C. Liu, *Anal. Chem.*, 2020, **92**, 6702–6708.
136 W. Tian, X. Liu, G. Wang and C. Liu, *Chem. Commun.*, 2020, **56**, 13445–13448.
137 X. Wang, X. Chen, C. Chu, Y. Deng, M. Yang, Z. Ji, F. Xu, D. Huo, Y. Luo and C. Hou, *Sens. Actuators, B*, 2020, **323**, 128653.
138 Y. Deng, G. Cao, X. Chen, M. Yang, D. Huo and C. Hou, *Talanta*, 2021, **232**, 122415.
139 C. Qian, R. Wang, H. Wu, F. Zhang, J. Wu and L. Wang, *Anal. Chem.*, 2019, **91**, 11362–11366.
140 K. Yin, X. Ding, Z. Li, H. Zhao, K. Cooper and C. Liu, *Anal. Chem.*, 2020, **92**, 8561–8568.
141 O. Mukama, J. Wu, Z. Li, Q. Liang, Z. Yi, X. Lu, Y. Liu, Y. Liu, M. Hussain and G. G. Makafe, *Biosens. Bioelectron.*, 2020, **159**, 112143.
142 Y. Chen, Y. Shi, Y. Chen, Z. Yang, H. Wu, Z. Zhou, J. Li, J. Ping, L. He and H. Shen, *Biosens. Bioelectron.*, 2020, **169**, 112642.
143 H. Wu, C. Qian, C. Wu, Z. Wang, D. Wang, Z. Ye, J. Ping, J. Wu and F. Ji, *Biosens. Bioelectron.*, 2020, **157**, 112153.
144 R. A. Lee, H. De Puig, P. Q. Nguyen, N. M. Angenent-Mari, N. M. Donghia, J. P. McGee, J. D. Dvorin, C. M. Klapperich, N. R. Pollock and J. J. Collins, *Proc. Natl. Acad. Sci. U. S. A.*, 2020, **117**, 25722–25731.
145 R. Zhou, Y. Li, T. Dong, Y. Tang and F. Li, *Chem. Commun.*, 2020, **56**, 3536–3538.
146 O. Mukama, T. Yuan, Z. He, Z. Li, J. de Dieu Habimana, M. Hussain, W. Li, Z. Yi, Q. Liang and L. Zeng, *Sens. Actuators, B*, 2020, **316**, 128119.
147 C. Qian, H. Wu, Y. Shi, J. Wu and H. Chen, *Sens. Actuators, B*, 2020, **305**, 127440.
148 B. Pang, J. Xu, Y. Liu, H. Peng, W. Feng, Y. Cao, J. Wu, H. Xiao, K. Pabbaraju and G. Tipples, *Anal. Chem.*, 2020, **92**, 16204–16212.
149 Z. Ali, R. Aman, A. Mahas, G. S. Rao, M. Tehseen, T. Marsic, R. Salunke, A. K. Subudhi, S. M. Hala and S. M. Hamdan, *Virus Res.*, 2020, **288**, 198129.
150 W. S. Zhang, J. Pan, F. Li, M. Zhu, M. Xu, H. Zhu, Y. Yu and G. Su, *Anal. Chem.*, 2021, **93**, 4126–4133.
151 Y. Jiang, M. Hu, A. Liu, Y. Lin, L. Liu, B. Yu, X. Zhou and D. Pang, *ACS Sens.*, 2021, **6**, 1086–1093.
152 H. Wu, Y. Chen, Y. Shi, L. Wang, M. Zhang, J. Wu and H. Chen, *Biosens. Bioelectron.*, 2021, **178**, 113001.
153 R. Wang, C. Qian, Y. Pang, M. Li, Y. Yang, H. Ma, M. Zhao, F. Qian, H. Yu and Z. Liu, *Biosens. Bioelectron.*, 2021, **172**, 112766.
154 R. Ding, J. Long, M. Yuan, X. Zheng, Y. Shen, Y. Jin, H. Yang, H. Li, S. Chen and G. Duan, *Int. J. Mol. Sci.*, 2021, **22**, 4842.
155 X. Wu, J. K. Tay, C. K. Goh, C. Chan, Y. H. Lee, S. L. Springs, K. S. Loh, T. K. Lu and H. Yu, *Biomaterials*, 2021, **274**, 120876.
156 K. H. Ooi, M. M. Liu, J. W. D. Tay, S. Y. Teo, P. Kaewsapsak, S. Jin, C. K. Lee, J. Hou, S. Maurer-Stroh and W. Lin, *Nat. Commun.*, 2021, **12**, 1–23.
157 M. Zhang, H. Wang, H. Wang, F. Wang and Z. Li, *Anal. Chem.*, 2021, **93**, 7942–7948.
158 Y. Zhang, M. Chen, C. Liu, J. Chen, X. Luo, Y. Xue, Q. Liang, L. Zhou, Y. Tao and M. Li, *Sens. Actuators, B*, 2021, **345**, 130411.
159 K. Yin, X. Ding, Z. Li, M. M. Sfeir, E. Ballesteros and C. Liu, *Lab Chip*, 2021, **21**, 2730–2737.
160 F. Chen, P. Lee, A. Y. Trick, J. S. Park, L. Chen, K. Shah, H. Mostafa, K. C. Carroll, K. Hsieh and T. Wang, *Biosens. Bioelectron.*, 2021, **190**, 113390.
161 X. Wu, C. Chan, S. L. Springs, Y. H. Lee, T. K. Lu and H. Yu, *Anal. Chim. Acta*, 2022, 339494.
162 T. Zhang, W. Zhao, X. Chen, X. Zhang, J. Zhu, S. Li, C. Wu, Z. Tian and G. Sui, *Anal. Chem.*, 2022, **94**, 15472–15480.
163 Y. Chen, X. Xu, J. Wang, Y. Zhang, W. Zeng, Y. Liu and X. Zhang, *Anal. Chem.*, 2022, **94**, 9724–9731.
164 H. Wu, X. Cao, Y. Meng, D. Richards, J. Wu, Z. Ye and A. J. deMello, *Biosens. Bioelectron.*, 2022, 114377.
165 M. Bao, S. Zhang, C. Ten Pas, S. J. Dollery, R. V. Bushnell, F. Yuqing, R. Liu, G. Lu, G. J. Tobin and K. Du, *Lab Chip*, 2022, **22**, 4849–4859.
166 Y. Tang, T. Song, L. Gao, S. Yin, M. Ma, Y. Tan, L. Wu, Y. Yang, Y. Wang and T. Lin, *Nat. Commun.*, 2022, **13**, 1–10.
167 Z. Xu, D. Chen, T. Li, J. Yan, J. Zhu, T. He, R. Hu, Y. Li, Y. Yang and M. Liu, *Nat. Commun.*, 2022, **13**, 1–14.
168 M. Hu, Z. Qiu, Z. Bi, T. Tian, Y. Jiang and X. Zhou, *Proc. Natl. Acad. Sci. U. S. A.*, 2022, **119**, e2202034119.
169 J. Liu, H. Wang, L. Zhang, Y. Lu, X. Wang, M. Shen, N. Li, L. Feng, J. Jing and B. Cao, *Small*, 2022, 2200854.
170 A. Ramachandran and J. G. Santiago, *Anal. Chem.*, 2021, **93**, 7456–7464.
171 J. Langer, D. Jimenez de Aberasturi, J. Aizpurua, R. A. Alvarez-Puebla, B. Auguié, J. J. Baumberg, G. C. Bazan, S. E. Bell, A. Boisen and A. G. Brolo, *ACS Nano*, 2019, **14**, 28–117.
172 D. W. Kimmel, G. LeBlanc, M. E. Meschievitz and D. E. Cliffel, *Anal. Chem.*, 2012, **84**, 685–707.
173 Z. Jin, D. Geißler, X. Qiu, K. D. Wegner and N. Hildebrandt, *Angew. Chem., Int. Ed.*, 2015, **54**, 10024–10029.
174 K. D. Wegner, Z. Jin, S. Linden, T. L. Jennings and N. Hildebrandt, *ACS Nano*, 2013, **7**, 7411–7419.
175 K. Shi, S. Xie, R. Tian, S. Wang, Q. Lu, D. Gao, C. Lei, H. Zhu and Z. Nie, *Sci. Adv.*, 2021, **7**, eabc7802.
176 R. Hajian, S. Balderston, T. Tran, T. DeBoer, J. Etienne, M. Sandhu, N. A. Wauford, J. Chung, J. Nokes and M. Athaiya, *Nat. Biomed. Eng.*, 2019, **3**, 427–437.

177 H. Li, J. Yang, G. Wu, Z. Weng, Y. Song, Y. Zhang, J. A. Vanegas, L. Avery, Z. Gao and H. Sun, *Angew. Chem., Int. Ed.*, 2022, **61**, e202203826.
178 P. Fozouni, S. Son, M. Díaz de León Derby, G. J. Knott, C. N. Gray, M. V. D'Ambrosio, C. Zhao, N. A. Switz, G. R. Kumar, S. I. Stephens and M. Ott, *Cell*, 2021, **184**, 323–333.e9.
179 T. Y. Liu, G. J. Knott, D. C. Smock, J. J. Desmarais, S. Son, A. Bhuiya, S. Jakhanwal, N. Prywes, S. Agrawal and M. Díaz de León Derby, *Nat. Chem. Biol.*, 2021, **17**, 982–988.
180 K. Guk, J. O. Keem, S. G. Hwang, H. Kim, T. Kang, E. Lim and J. Jung, *Biosens. Bioelectron.*, 2017, **95**, 67–71.
181 H. Kim, S. Lee, H. W. Seo, B. Kang, J. Moon, K. G. Lee, D. Yong, H. Kang, J. Jung and E. Lim, *ACS Nano*, 2020, **14**, 17241–17253.
182 S. Balderston, J. J. Taulbee, E. Celaya, K. Fung, A. Jiao, K. Smith, R. Hajian, G. Gasiunas, S. Kutanovas and D. Kim, *Nat. Biomed. Eng.*, 2021, 1–13.
183 Y. Dai, R. A. Somoza, L. Wang, J. F. Welter, Y. Li, A. I. Caplan and C. C. Liu, *Angew. Chem.*, 2019, **131**, 17560–17566.
184 D. Zhang, Y. Yan, H. Que, T. Yang, X. Cheng, S. Ding, X. Zhang and W. Cheng, *ACS Sens.*, 2020, **5**, 557–562.
185 Z. Li, X. Ding, K. Yin, Z. Xu, K. Cooper and C. Liu, *Biosens. Bioelectron.*, 2021, **192**, 113498.
186 Y. Lee, J. Choi, H. Han, S. Park, S. Y. Park, C. Park, C. Baek, T. Lee and J. Min, *Sens. Actuators, B*, 2021, **326**, 128677.
187 Y. Pang, Q. Li, C. Wang, Z. Sun and R. Xiao, *Chem. Eng. J.*, 2022, **429**, 132109.
188 J. Choi, J. Lim, M. Shin, S. Paek and J. Choi, *Nano Lett.*, 2020, **21**, 693–699.
189 R. Zeng, W. Wang, M. Chen, Q. Wan, C. Wang, D. Knopp and D. Tang, *Nano Energy*, 2021, **82**, 105711.
190 C. Wang, C. Han, X. Du and W. Guo, *Anal. Chem.*, 2021, **93**, 12881–12888.
191 D. Y. Zhang, A. J. Turberfield, B. Yurke and E. Winfree, *Science*, 2007, **318**, 1121–1125.
192 T. Tian, B. Shu, Y. Jiang, M. Ye, L. Liu, Z. Guo, Z. Han, Z. Wang and X. Zhou, *ACS Nano*, 2020, **15**, 1167–1178.
193 S. Son, A. Lyden, J. Shu, S. I. Stephens, P. Fozouni, G. J. Knott, D. C. Smock, T. Y. Liu, D. Boehm, C. Simoneau and D. A. Fletcher, *medRxiv*, 2021, preprint, DOI: **10.1101/2021.08.02.21261509**.
194 R. Bruch, J. Baaske, C. Chatelle, M. Meirich, S. Madlener, W. Weber, C. Dincer and G. A. Urban, *Adv. Mater.*, 2019, **31**, 1905311.
195 T. Zhou, R. Huang, M. Huang, J. Shen, Y. Shan and D. Xing, *Adv. Sci.*, 2020, **7**, 1903661.
196 R. Bruch, M. Johnston, A. Kling, T. Mattmüller, J. Baaske, S. Partel, S. Madlener, W. Weber, G. A. Urban and C. Dincer, *Biosens. Bioelectron.*, 2021, **177**, 112887.
197 T. Tian, B. Shu, Y. Jiang, M. Ye, L. Liu, Z. Guo, Z. Han, Z. Wang and X. Zhou, *ACS Nano*, 2021, **15**, 1167–1178.
198 H. Shinoda, Y. Taguchi, R. Nakagawa, A. Makino, S. Okazaki, M. Nakano, Y. Muramoto, C. Takahashi, I. Takahashi and J. Ando, *Commun. Biol.*, 2021, **4**, 1–7.
199 Y. Cui, S. Fan, Z. Yuan, M. Song, J. Hu, D. Qian, D. Zhen, J. Li and B. Zhu, *Talanta*, 2021, **224**, 121878.
200 I. A. Iwe, W. Li, Z. Li and J. Huang, *Talanta*, 2021, **226**, 122146.
201 Y. Zhang, L. Qian, W. Wei, Y. Wang, B. Wang, P. Lin, W. Liu, L. Xu, X. Li and D. Liu, *ACS Synth. Biol.*, 2017, **6**, 211–216.
202 H. Lee, J. Choi, E. Jeong, S. Baek, H. C. Kim, J. Chae, Y. Koh, S. W. Seo, J. Kim and S. J. Kim, *Nano Lett.*, 2018, **18**, 7642–7650.
203 J. Moon, H. Kwon, D. Yong, I. Lee, H. Kim, H. Kang, E. Lim, K. Lee, J. Jung and H. G. Park, *ACS Sens.*, 2020, **5**, 4017–4026.
204 K. N. Hass, M. Bao, Q. He, L. Liu, J. He, M. Park, P. Qin and K. Du, *ACS Omega*, 2020, **5**, 27433–27441.
205 W. Xu, T. Jin, Y. Dai and C. C. Liu, *Biosens. Bioelectron.*, 2020, **155**, 112100.
206 Q. He, D. Yu, M. Bao, G. Korensky, J. Chen, M. Shin, J. Kim, M. Park, P. Qin and K. Du, *Biosens. Bioelectron.*, 2020, **154**, 112068.
207 X. Yang, J. Li, S. Zhang, C. Li and J. Ma, *Anal. Chem.*, 2022, **94**, 13076–13083.
208 M. Zeng, Y. Ke, Z. Zhuang, C. Qin, L. Y. Li, G. Sheng, Z. Li, H. Meng and X. Ding, *Anal. Chem.*, 2022, **94**, 10805–10812.
209 T. Luo, J. Li, Y. He, H. Liu, Z. Deng, X. Long, Q. Wan, J. Ding, Z. Gong and Y. Yang, *Anal. Chem.*, 2022, **94**, 6566–6573.
210 C. M. Green, J. Spangler, K. Susumu, D. A. Stenger, I. L. Medintz and S. A. Díaz, *ACS Nano*, 2022, **16**, 20693–20704.
211 Z. Chen, J. Li, T. Li, T. Fan, C. Meng, C. Li, J. Kang, L. Chai, Y. Hao and Y. Tang, *Natl. Sci. Rev.*, 2022, **9**, nwac104.
212 P. Qin, M. Park, K. J. Alfson, M. Tamhankar, R. Carrion, J. L. Patterson, A. Griffiths, Q. He, A. Yildiz and R. Mathies, *ACS Sens.*, 2019, **4**, 1048–1054.
213 Q. Chen, T. Tian, E. Xiong, P. Wang and X. Zhou, *Anal. Chem.*, 2019, **92**, 573–577.
214 J. Li, L. Tang, T. Li, K. Li, Y. Zhang, W. Ni, M. Xiao, Y. Zhao, Z. Zhang and G. Zhang, *ACS Sens.*, 2022, **7**, 2680–2690.
215 C. Zhang, P. Zhang, H. Ren, P. Jia, J. Ji, L. Cao, P. Yang, Y. Li, J. Liu and Z. Li, *Chem. Eng. J.*, 2022, **446**, 136864.
216 H. Shinoda, T. Iida, A. Makino, M. Yoshimura, J. Ishikawa, J. Ando, K. Murai, K. Sugiyama, Y. Muramoto and M. Nakano, *Commun. Biol.*, 2022, **5**, 1–8.
217 M. Broto, M. M. Kaminski, C. Adrianus, N. Kim, R. Greensmith, S. Dissanayake-Perera, A. J. Schubert, X. Tan, H. Kim and A. S. Dighe, *Nat. Nanotechnol.*, 2022, **17**, 1120–1126.
218 J. Yang, Y. Song, X. Deng, J. A. Vanegas, Z. You, Y. Zhang, Z. Weng, L. Avery, K. D. Dieckhaus and A. Peddi, *Nat. Chem. Biol.*, 2022, 1–10.
219 S. Dube, J. Qin and R. Ramakrishnan, *PLoS One*, 2008, **3**, e2876.
220 C. M. Hindson, J. R. Chevillet, H. A. Briggs, E. N. Gallichotte, I. K. Ruf, B. J. Hindson, R. L. Vessella and M. Tewari, *Nat. Methods*, 2013, **10**, 1003–1005.
221 J. S. Park, K. Hsieh, L. Chen, A. Kaushik, A. Y. Trick and T. Wang, *Adv. Sci.*, 2021, **8**, 2003564.
222 S. Teh, R. Lin, L. Hung and A. P. Lee, *Lab Chip*, 2008, **8**, 198–220.

223 J. Wang, W. Yu, Z. Wu, X. Liu and Y. Chen, *Appl. Phys. Lett.*, 2022, **120**, 204101.
224 W. Trypsteen, M. Vynck, J. De Neve, P. Bonczkowski, M. Kiselinova, E. Malatinkova, K. Vervisch, O. Thas, L. Vandekerckhove and W. De Spiegelaere, *Anal. Bioanal. Chem.*, 2015, **407**, 5827–5834.
225 X. Luo, Y. Xue, E. Ju, Y. Tao, M. Li, L. Zhou, C. Yang, J. Zhou and J. Wang, *Anal. Chim. Acta*, 2022, **1192**, 339336.
226 J. Q. Cui, B. Cui, F. X. Liu, Y. Lin and S. Yao, *Sens. Actuators, B*, 2022, 132573.
227 Z. Yu, L. Xu, W. Lyu and F. Shen, *Lab Chip*, 2022, **22**, 2954–2961.
228 C. H. Y. Chung, B. Cui, R. Song, X. Liu, X. Xu and S. Yao, *Micromachines*, 2019, **10**, 592.
229 R. Dangla, S. C. Kayi and C. N. Baroud, *Proc. Natl. Acad. Sci. U. S. A.*, 2013, **110**, 853–858.
230 X. Xu, H. Yuan, R. Song, M. Yu, H. Y. Chung, Y. Hou, Y. Shang, H. Zhou and S. Yao, *Biomicrofluidics*, 2018, **12**, 014103.
231 C. Sun, L. Liu, H. N. Vasudevan, K. Chang and A. R. Abate, *Anal. Chem.*, 2021, **93**, 9974–9979.
232 X. Lin, X. Huang, K. Urmann, X. Xie and M. R. Hoffmann, *ACS Sens.*, 2019, **4**, 242–249.
233 J. E. Kreutz, J. Wang, A. M. Sheen, A. M. Thompson, J. P. Staheli, M. R. Dyen, Q. Feng and D. T. Chiu, *Lab Chip*, 2019, **19**, 1035–1040.
234 Z. Yu, W. Lyu, M. Yu, Q. Wang, H. Qu, R. F. Ismagilov, X. Han, D. Lai and F. Shen, *Biosens. Bioelectron.*, 2020, **155**, 112107.
235 M. Shehadul Islam, A. Aryasomayajula and P. R. Selvaganapathy, *Micromachines*, 2017, **8**, 83.
236 M. A. Lalli, J. S. Langmade, X. Chen, C. C. Fronick, C. S. Sawyer, L. C. Burcea, M. N. Wilkinson, R. S. Fulton, M. Heinz and W. J. Buchser, *Clin. Chem.*, 2021, **67**, 415–424.
237 M. Alafeef, P. Moitra, K. Dighe and D. Pan, *Nat. Protoc.*, 2021, **16**, 3141–3162.
238 S. A. Byrnes, R. Gallagher, A. Steadman, C. Bennett, R. Rivera, C. Ortega, S. T. Motley, P. Jain, B. H. Weigl and J. T. Connelly, *Anal. Chem.*, 2021, **93**, 4160–4165.
239 B. A. Rabe and C. Cepko, *Proc. Natl. Acad. Sci. U. S. A.*, 2020, **117**, 24450–24458.
240 S. Agrawal, A. Fanton, S. S. Chandrasekaran, B. Charrez, A. M. Escajeda, S. Son, R. Mcintosh, A. Bhuiya, M. Díaz de León Derby and N. A. Switz, *medRxiv*, 2021, preprint, DOI: **10.1101/2020.12.14.20247874**.
241 J. Arizti-Sanz, A. Bradley, Y. B. Zhang, C. K. Boehm, C. A. Freije, M. E. Grunberg, T. F. Kosoko-Thoroddsen, N. L. Welch, P. P. Pillai and S. Mantena, *Nat. Biomed. Eng.*, 2022, 1–12.
242 H. Gong, I. Holcomb, A. Ooi, X. Wang, D. Majonis, M. A. Unger and R. Ramakrishnan, *Bioconjugate Chem.*, 2016, **27**, 217–225.
243 P. Zhang, L. Chen, J. Hu, A. Y. Trick, F. Chen, K. Hsieh, Y. Zhao, B. Coleman, K. Kruczynski and T. R. Pisanic II, *Biosens. Bioelectron.*, 2022, **195**, 113656.
244 I. Lee, S. Kwon, M. Sorci, P. S. Heeger and J. S. Dordick, *Anal. Chem.*, 2021, **93**, 16528–16534.
245 J. Ko, Y. Wang, J. C. Carlson, A. Marquard, J. Gungabeesoon, A. Charest, D. Weitz, M. J. Pittet and R. Weissleder, *Adv. Biosyst.*, 2020, **4**, 1900307.
246 J. Shen, X. Zhou, Y. Shan, H. Yue, R. Huang, J. Hu and D. Xing, *Nat. Commun.*, 2020, **11**, 1–10.
247 C. Niu, C. Wang, F. Li, X. Zheng, X. Xing and C. Zhang, *Biosens. Bioelectron.*, 2021, **183**, 113196.
248 C. Li, B. Zheng, Y. Liu, J. Gao, M. Zheng, D. Pang and H. Tang, *Biosens. Bioelectron.*, 2020, **169**, 112650.
249 C. Li, B. Zheng, J. Li, J. Gao, Y. Liu, D. Pang and H. Tang, *ACS Nano*, 2021, **15**, 8142–8154.
250 P. Wu, X. Ye, D. Wang, F. Gong, X. Wei, S. Xiang, J. Zhang, T. Kai and P. Ding, *J. Hazard. Mater.*, 2022, **424**, 127690.
251 X. Zhao, L. Zeng, Q. Mei and Y. Luo, *ACS Sens.*, 2020, **5**, 2239–2246.
252 Y. Xiong, J. Zhang, Z. Yang, Q. Mou, Y. Ma, Y. Xiong and Y. Lu, *J. Am. Chem. Soc.*, 2019, **142**, 207–213.
253 C. Zhang, H. Yao, Q. Ma and B. Yu, *Analyst*, 2021, **146**, 6576–6581.
254 J. Li, S. Yang, C. Zuo, L. Dai, Y. Guo and G. Xie, *ACS Sens.*, 2020, **5**, 970–977.
255 A. Mahas, Q. Wang, T. Marsic and M. M. Mahfouz, *Anal. Chem.*, 2022, **94**, 4617–4626.
256 M. Liang, Z. Li, W. Wang, J. Liu, L. Liu, G. Zhu, L. Karthik, M. Wang, K. Wang and Z. Wang, *Nat. Commun.*, 2019, **10**, 1–9.
257 R. S. Iwasaki and R. T. Batey, *Nucleic Acids Res.*, 2020, **48**, e101.
258 J. Zhao, Z. Tan, L. Wang, C. Lei and Z. Nie, *Chem. Commun.*, 2021, **57**, 7051–7054.
259 C. Zhang, H. Yao, Q. Ma and B. Yu, *Analyst*, 2021, **146**, 6576–6581.